# Y-complex nucleoporins independently contribute to nuclear pore assembly and gene regulation in neuronal progenitors

Clarisse Orniacki, Annalisa Verrico, Stéphane Pelletier, Benoit Souquet, Fanny Coulpier, Laurent Jourdren, Serena Benetti, Valérie Doye

# Y-complex nucleoporins independently contribute to nuclear pore assembly and gene regulation in neuronal progenitors

Clarisse Orniacki[1-2], Annalisa Verrico[1], Stéphane Pelletier[1], Benoit Souquet[1,#], Fanny Coulpier[3], Laurent Jourdren[3,] Serena Benetti[1] and Valérie Doye[1]

[1] Université Paris Cité, CNRS, Institut Jacques Monod, F-75013 Paris, France

[2] Ecole Doctorale BioSPC, Université Paris Cité, Paris, France

[3] GenomiqueENS, Institut de Biologie de l'ENS (IBENS), Département de biologie, École normale supérieure, CNRS, INSERM, Université PSL, 75005 Paris, France

*Corresponding author and lead contact: valerie.doye@ijm.fr

[#] Present address: Ophthalmology Department, A. de Rothschild Foundation Hospital, 75019 Paris, France

**Keywords:** Nucleoporin, Nup133, Seh1, neuronal progenitors, Nup210L, Lhx1

**Running title:** Y-Nups in mESC differentiation

## SUMMARY STATEMENT

We report roles for the Y-complex nucleoporins Nup133 and Seh1 in gene regulation upon neuroectodermal differentiation and show that this process can be uncoupled from nuclear pore basket integrity.


## ABSTRACT

Besides assembling nuclear pore complexes, the conduits of nuclear transport, many nucleoporins also contribute to chromatin organization and gene expression, with critical roles in development and pathologies. We previously reported that Nup133 and Seh1, two components of the Y-complex subassembly of the nuclear pore scaffold, are dispensable for mouse embryonic stem cell viability but required for their survival during neuroectodermal differentiation. Here, a transcriptomic analysis revealed that Nup133 regulates a subset of genes at early stages of neuroectodermal differentiation, including *Lhx1 and Nup210L*, encoding a newly validated nucleoporin. These genes are also misregulated in *Nup133ΔMid* neuronal progenitors, in which nuclear pore basket assembly is impaired. However, a four-fold reduction of Nup133, despite also affecting basket assembly, is not sufficient to alter *Nup210L* and *Lhx1* expression. Finally, these two genes are also misregulated in *Seh1*-deficient neural progenitors only showing a mild reduction in nuclear pore density. Together these data reveal a shared function of Y-complex nucleoporins in gene regulation during neuroectodermal differentiation, apparently independent of nuclear pore basket integrity.

## INTRODUCTION

As channels embedded in the nuclear envelope, the nuclear pore complexes (NPCs) constitute the only gateway for selective transport of macromolecules between the cytoplasm and the nucleus. These impressive structures are composed of proteins called nucleoporins (Nups) that assemble in a highly organized and modular manner (reviewed in Dultz et al., (2022)). The Y-complex - also named Nup107-160 complex - that comprises in vertebrates nine distinct proteins, is a key structural subunit of the NPC scaffold. 16 copies of this complex assemble on the nuclear and cytoplasmic sides of the NPC to build up its outer rings, to which cytoplasmic filaments and the nuclear basket are anchored.

In addition to their canonical nuclear transport function, many Nups are also known to have other cellular functions, notably in cell cycle progression or as key regulators of chromatin organization and gene expression (reviewed in Buchwalter et al., 2019; Hezwani and Fahrenkrog, 2017). In line with these multiple functions, mutations in many Nups have been identified as primary causes of rare genetic diseases. Despite the presence of NPCs in all nucleated cells, most of these diseases specifically affect one or a few organs (reviewed in Jühlen and Fahrenkrog, 2018). Such tissue or cell-type specific alterations may reflect variable Nup stoichiometry at NPCs, as notably reported for several integral membrane Nups and peripheral Nups (Ori et al., 2013). For instance, increased levels of the transmembrane protein Nup210 in myoblasts and neuronal progenitors was shown to be critical for their differentiation (D'Angelo et al., 2012). Likewise, depletion of the basket nucleoporin Nup50 reduces the differentiation efficiency of C2C12 myoblasts (Buchwalter et al., 2014). In contrast, another basket nucleoporin, Nup153, which is highly expressed in pluripotent cells and neuronal progenitors compared to differentiated cells, is required for the maintenance of their identities, notably by regulating epigenetic gene silencing and transcriptional programs (Jacinto et al., 2015; Toda et al., 2017). More recently, the Y-complex constituent Seh1, which is highly expressed in oligodendrocyte progenitor cells, was shown to be required for oligodendrocyte differentiation and myelination by regulating the assembly of a transcription complex at the nuclear periphery (Liu et al., 2019). However, individual Y-complex Nups also contribute to earlier stages of differentiation, as underscored by the impaired neuroectodermal differentiation of *Nup133*$^{-/-}$, *Seh1*$^{-/-}$ and *Nup43*$^{-/-}$ mouse embryonic stem cells (mESCs) (Gonzalez-Estevez, Verrico et al., 2021; Lupu et al., 2008).

Earlier studies had found that the vertebrate Y-complex is, as an entity, critically required for NPC assembly both at the end of mitosis and during interphase (Doucet and Hetzer, 2010; Harel et al., 2003; Vollmer et al., 2015; Walther et al., 2003). The viability of *Nup133*$^{-/-}$, *Seh1*$^{-/-}$ and *Nup43*$^{-/-}$ mESCs however indicated that the corresponding Y-complex Nups were individually largely dispensable for nuclear pore assembly in these pluripotent cells. Consistently, we previously showed that mutations of Nups that form the short arm of the Y-complex, namely Nup43, Nup85 and Seh1, only lead to a mild decrease in NPC density in pluripotent mESCs (Gonzalez-Estevez, Verrico et al., 2021). In contrast, pluripotent *Nup133*$^{-/-}$ mESCs feature a normal NPC density, but show specific nuclear basket defects, with half of NPCs lacking Tpr while Nup153 dynamics was increased (Souquet et al., 2018). How Y-complex Nups contribute to NPC assembly in differentiating mESCs was unknown.

Because of the established implication of the basket nucleoporins Nup153 and Tpr in chromatin organization and gene regulation (Aksenova et al., 2020; Boumendil et al., 2019; Jacinto et al., 2015; Krull et al., 2010; Toda et al., 2017), we decided to investigate potential gene expression defects in *Nup133*$^{-/-}$ mESCs during neuroectodermal differentiation. Here we show that Nup133 regulates a subset of genes, including *Lhx1* and *Nup210L* that are similarly misregulated in the absence of Seh1. However, *Nup133* and *Seh1* deficiencies display distinct NPC assembly phenotypes in neuronal progenitors, thus indicating separate roles for these proteins in NPC architecture and gene regulation in the context of mESC differentiation.

## RESULTS

### Nup133 is required for the regulation of a subset of genes during neuroectodermal differentiation

We first determined if the impaired differentiation of *Nup133*$^{-/-}$ mESCs, initially described in cells derived from *merm* (behaving as *Nup133*$^{-/-}$) blastocysts (Lupu et al. 2008), was also observed in an independent genetic background. As Lupu and colleagues, we observed altered growth and increased cell death upon neuroectodermal differentiation of *Nup133*$^{-/-}$ mESCs derived by CRISPR/Cas9-editing from HM1 mESCs (previously described in Souquet et al., 2018) (**Fig. 1A,B**). To evaluate the potential effect of Nup133 deficiency in gene regulation upon neuroectodermal differentiation, we assessed the mRNA levels of genes expressed in pluripotent cells (*Oct4* and *Nanog*) and in early neuronal progenitors (*Sox1* and *Pax6*) that are considered markers for the respective states. RT-qPCR analyses showed that these genes were properly repressed and activated, respectively, in *Nup133*$^{-/-}$ cells stimulated to differentiate towards neuroectoderm (**Fig. 1C**). This indicated that despite their impaired viability at early stages of differentiation (**Fig. 1A, B**) the surviving *Nup133*$^{-/-}$ cells are able to exit pluripotency and to commit towards the neuronal lineage, without overt defects in the expression of these markers.

To more broadly explore the impact of Nup133 on gene expression, we compared the transcriptome of *WT* and *Nup133*$^{-/-}$ mESCs at the pluripotent state and after 2 or 3 days of differentiation towards neuroectodermal lineage. We therefore used *WT* and *Nup133*$^{-/-}$ mouse cell lines from two distinct genetic backgrounds, namely the 129/ola blastocyst-derived HM1 control cell line (Selfridge et al., 1992) and its isogenic CRISPR/Cas9-edited *Nup133*$^{-/-}$ derivatives (#14 and #19; Souquet et al., 2018), and the 129/Sv blastocyst-derived control (#1A4) and *Nup133* mutant$^{-}$ (*merm*, #319) mESC lines (Lupu et al., 2018) (**Table S1**). This analysis revealed that the transcriptomes of pluripotent *WT* and *Nup133*$^{-/-}$ mESCs were overall similar, with 43 down- and only 2 up-regulated genes, based on an adjusted p-value<0.05 and a |logFold Change|>2, whereas an increasing number of genes were misregulated (and notably upregulated) at day 3 of differentiation, with 57 down- and 61 up-regulated genes, using the same cutoffs (**Figs. 1D and S1A**).

We assayed by RT-qPCR the altered expression of a subset of these genes, filtered by criteria of differential expression (log2FC>2 or <-2), significance (adjusted p-value<0.05) and lastly by

average expression level (average number of reads with a log2(CPM)>1, to ensure proper detection by RT-qPCR) (**Fig. S1B-E**). In addition to *WT (HM1)* and *Nup133*$^{-/-}$ (#14) used for the initial RNA-seq experiment, these analyses were also conducted on samples from *Nup133* "*Rescue*" cell lines generated by inserting the GFP-Nup133 transgene in *Nup133*$^{-/-}$ (#14) mESCs at the permissive *Tigre* locus (Zeng et al., 2008). As an additional control, we used an HM1-derived cell line that carries a transgene (*OsTIR*) similarly inserted in the *Tigre* locus (**Fig. S2A and Table S1**). In contrast to the impaired viability of *Nup133*$^{-/-}$ mESCs upon neuroectodermal differentiation, the survival of the *Rescue* and *WT (OsTIR)* cell lines were similar, confirming the functionality of the GFP-Nup133 transgene (**Fig. 2A-C)**.

For the candidate genes localized on the short arm of the Y chromosome (*Ddx3y* and *Eif2s3y,* also located in close proximity to the loci of *Uty, Uba1y, Kdm5d and Zfy* (Subrini and Turner, 2021)) we observed clone-dependent expression variations (**Fig. S1B)**. This suggests that their apparent shared misregulations, also reported in *Tet1* and *Tet2* mutant mESCs (Huang et al., 2013), might be in our case caused by partial loss or silencing of this genomic region, independently of *Nup133* deficiency.

In contrast, we could validate the increased mRNA levels *in Nup133*$^{-/-}$ compared to *WT* of *Nuggc* at day 0*,* and of *Nup210L* and *Lhx1* at day 3 of differentiation (**Fig. S1C**). We also confirmed the reduced mRNA levels in *Nup133*$^{-/-}$ compared to *WT* for *Magohb* and *Wfikkn1* (but not *Acta2*) at day 3 of differentiation (**Fig. S1D**). Finally, reduced mRNA levels of the assayed candidate genes at the pluripotent state (day 0) were not significant due to high variability among replicates or between control cell lines (HM1 and OsTIR) (**Fig. S1E**). Importantly, among the validated candidate genes, *Lhx1, Nup210L*, *Nuggc* and *Magohb* were all efficiently restored to wild-type levels by the *GFP-Nup133* transgene.

*Lhx1* is a transcription factor involved in kidney and brain differentiation (Costello et al., 2015; Delay et al., 2018; McMahon et al., 2019; Shawlot et al., 1999), two organs affected in rare genetic diseases linked to *Nup133* mutations, namely steroid-resistant nephrotic syndrome and Galloway Mowat syndrome (Braun et al., 2018; Fujita et al., 2018). We further focused on this gene because of its complex misregulation in *Nup133*$^{-/-}$ cells. Indeed, while we confirmed by RT-qPCR the upregulation of *Lhx1* expression at day 3 of differentiation

(**Fig. S1C**), *Lhx1* was subsequently downregulated again at later time-points (days 5 and 7 of differentiation) in *Nup133*$^{-/-}$ cells compared to *WT* and *Rescue* cells (**Fig. 2D**).

The other candidate gene we further characterized, *Nup210L,* is the differentially expressed gene (DEG) with the most significant p-value at day 3 of differentiation (**Fig. 1D**). It is also one of the rare DEGs whose expression already increased at day 2 compared to *WT* cells (**Fig. S1A**). In mice, *Nup210L* mRNA is mainly detected in the testis and to a lesser extent in the embryonic brain (https://www.ncbi.nlm.nih.gov/gene/77595); in humans, besides testis, *Nup210L* expression was also detected in the prefrontal cortex neurons of rare individuals (Gusev et al., 2019). Analyses at later stages (day 5 and 7) of differentiation towards neuroectoderm showed that *Nup210L* was still more expressed in *Nup133*$^{-/-}$ compared to *WT* and *Rescue* cells, although a progressive increase of its expression was also observed in the latter cell lines (**Fig. 2E**).

As its name implies, *Nup210L* encodes a potential homologue of the transmembrane nucleoporin Nup210/gp210 with 43% overall amino acid identity between the two proteins (**Fig. 2F**). However, its putative NPC localization had never been established. To address this issue, we generated a GFP-tagged construct encompassing the minimal NPC targeting determinants previously established for gp210/Nup210 (Wozniak and Blobel, 1992), namely Nup210L predicted signal peptide, transmembrane domain and C-terminal domain (**Fig. 2F**). This Nup210L-mini construct when expressed at low levels in mESCs is targeted to the nuclear envelope where it colocalizes with the nucleoporin Tpr. This indicates that, like its homolog, Nup210L is indeed a nucleoporin (**Fig. 2F**).

**The middle-domain of Nup133 is required for mESC differentiation, gene regulation and nuclear basket assembly in neuronal progenitors**

Having established the requirement of Nup133 for cell viability upon differentiation and for the regulation of a subset of genes, we next aimed to determine how Nup133 contributes to these processes. We first focused on the middle domain of Nup133 that is necessary for the proper assembly of the nuclear pore basket in pluripotent mESCs (Souquet et al., 2018). We therefore integrated the pCAG-GFP-Nup133Δmid transgene in HM1-derived *Nup133*$^{-/-}$ mESCs at the *Tigre* locus (**Fig. S2A**). The GFP-Nup133Δmid protein levels in the resulting *Nup133Δmid* cells were comparable to those of endogenous Nup133 and of GFP-Nup133 in the *Rescue* cell lines throughout differentiation (**Fig. 2B**). Cell counts upon monolayer

differentiation towards neuroectodermal lineage showed for the *Nup133Δmid* cell lines a viability phenotype intermediate between *WT* and *Nup133*$^{-/-}$, indicating that the middle domain of Nup133 is required for some, but not all, of the functions of this nucleoporin upon differentiation (**Fig. 2C**).

In contrast, RT-qPCR analysis showed that *Nup210L* and *Lhx1* were similarly misregulated upon neuronal differentiation in *Nup133Δmid* and in *Nup133*$^{-/-}$ cells (**Fig. 2D and E**).

The improved survival upon differentiation of *Nup133Δmid* compared to *Nup133*$^{-/-}$ cells enabled us to perform immunofluorescence analyses to determine whether the NPC basket assembly defects, previously observed in pluripotent mESCs lacking Nup133 or its middle domain, also occurred at the differentiated stage. Quantitative immunofluorescence analyses, performed after 5 days of differentiation, showed that the intensity of Tpr at the nuclear envelope was comparable between the *WT* and *Rescue* cell lines. In contrast, a two-fold decrease was observed in *Nup133Δmid* neuronal progenitors (**Fig. 3A, B**), a defect comparable to the one previously observed at the pluripotent state (Souquet et al., 2018). In addition, we also measured an increased Nup153 intensity at the nuclear envelope in *Nup133Δmid* progenitors compared to neuronal progenitors from *WT* or *Rescue* cell lines (**Fig. 3C**). This increased level of Nup153 is unlikely to solely reflect a global increase in NPC number as reported upon Tpr depletion in other cell lines (McCloskey et al., 2018), since similar quantifications revealed a milder increase of Nup98 intensity at the nuclear envelope compared to Nup153 (**Fig. 3D**). Likewise, an increased accessibility of the Nup153 epitope when Tpr is absent seems unlikely, as such an effect was not previously observed in Nup133$^{-/-}$ mESCs at the pluripotent stage (Souquet et al., 2018). The high level of Nup153 observed may therefore reflect an increased stoichiometry of Nup153 per NPC in *Nup133Δmid*-compared to control-derived neuronal progenitors, possibly reflecting different stages of differentiation as previously described (Toda et al., 2017).

**Nup133-dependent gene regulation and nuclear basket assembly can be uncoupled**

Having identified a critical function for the middle domain of Nup133 in gene regulation, we next aimed to determine the levels of Nup133 required for this process. We therefore established *Nup133-degron* cell lines that allow auxin-mediated degradation of a GFP-tagged allele of *Nup133* in an OsTIR-expressing mESC line (Gonzalez-Estevez, Verrico et al., (2021), see Materials and Methods and **Fig. S2B**).

The resulting *Nup133-degron* cell lines maintained normal *Nup133* mRNA expression during differentiation (**Fig. S3A**), but actual Nup133 protein levels (without Auxin treatment) were only ~25% of that found in *WT* cells (**Figs. 4A and S3B**). This could be due to leaky OsTIR-induced degradation as previously reported (Mendoza-Ochoa et al., 2019; Yesbolatova et al., 2020), decreased stability of the tagged nucleoporin, or impaired export or translation of its mRNA. Nevertheless, these cells properly differentiated in the absence of auxin (**Figs. 4C**, **S3D** and **S3E**). As anticipated, addition of auxin to the medium throughout differentiation led to a *Nup133*$^{-/-}$-like phenotype: normal growth at the pluripotent state but massive cell death in neuronal differentiation (**Figs. 4C, S3C** and **S3D**).

Importantly, the lower Nup133 levels observed in the degron cell lines in the absence of auxin was not accompanied by the altered expression of *Nup210L* or *Lhx1* during neuronal differentiation (**Fig. 4E**). In contrast, more extensive depletion of Nup133 upon continuous auxin treatment mimicked the effect of *Nup133* inactivation on these genes (**Fig. 4E**).

Quantification of the nuclear basket protein Tpr in the *Nup133-degron* cell lines revealed that, even in the absence of auxin, Tpr levels at the nuclear envelope were already reduced to ~60% of the WT levels both in pluripotent cells and in neuronal progenitors (**Figs. 4D** and **S4A**). In contrast, the levels of Nup98 were not reduced in *Nup133-degron* cells (**Fig. S4C**), consistent with a largely unaltered NPC density and a specific alteration of the nuclear basket. The minor - i.e., less than 10% - increase in Nup98 intensity observed in one of the two cell lines (*Nup133-degron* #1) may reflect modest clonal-dependent variations of NPC density. Finally, the levels of Nup153 were very mildly increased only in the *Nup133-degron* #1 cells, with a similar trend in both undifferentiated and differentiated cells (**Fig. S4B,D**). These results indicate that a 4-fold reduction of Nup133 protein levels in untreated *Nup133-degron cells* is sufficient to severely impair Tpr recruitment or stabilization at nuclear pores, without major additional impact on NPC density.

Finally, although most of the GFP-mAID-Nup133 protein was already degraded after 30 minutes of auxin treatment in differentiated cells (**Fig. 4B**), a 16 to 24h auxin treatment of these cells only led to a modest additional decrease of Tpr levels at the nuclear envelope compared to the untreated *Nup133-degron* cells (**Figs. 4D** and **S4A**).

Overall, these results thus demonstrated that a correct Nup133 stoichiometry is critical for nuclear basket assembly, yet is not required for cell viability or gene regulation upon neuroectodermal differentiation. Taken together these data also reveal that a properly

assembled nuclear basket at all NPCs is not required to regulate the expression of Nup133-target genes.

***Nup210L* mRNA levels rapidly increase in response to Nup133 or Seh1 depletion.**

We next aimed to determine if the altered expression of *Nup210L* and *Lhx1* was specific for Nup133 or was shared by other Y-complex constituents. In view of the requirement for Seh1 in global NPC assembly, distinct from the specific basket assembly defect of *Nup133* mutant cells (Gonzalez-Estevez, Verrico et al., 2021), we chose to assess its implication at early stages of differentiation. Despite a very extensive death of the *Seh1*$^{-/-}$ mutant cells upon differentiation, (Gonzalez-Estevez, Verrico et al., 2021), we could recover some mRNAs from these cells at day 3 of differentiation. As observed for *Nup133*$^{-/-}$ mESCs (**Fig. 1A**), *Seh1*$^{-/-}$ cells properly repressed pluripotency markers and were able to induce early differentiation markers (**Fig. S5A**). Importantly, mRNA levels of both *Nup210L* and *Lhx1* were aberrantly increased in *Seh1*$^{-/-}$ cells at day 3 of differentiation as also observed in differentiating *Nup133*$^{-/-}$ cells (**Fig. 5A**).

The low viability of *Seh1*$^{-/-}$ cells upon differentiation (Gonzalez-Estevez, Verrico et al., 2021) did not allow us to perform quantitative immunofluorescence studies at the differentiated stage. We therefore established and validated new *Seh1-degron* cell lines (see Materials and Methods **and Fig. S2C**), in which the C-terminally-tagged form of Seh1 was properly and homogeneously expressed upon differentiation (**Figs. 5B** and **S5B,C**). In the resulting *Seh1-degron* cells, 24h addition of auxin at day 2 or 4 of differentiation led to impaired viability of the cells (**Fig. 5C**). This indicates that Seh1 is not solely required at the early onset of neuronal progenitor differentiation, but also for the proper growth or viability of the progenitors themselves. Analyses of nuclear pore assembly in *Seh1-degron*-derived neuronal progenitors (at day 5 of differentiation) did not reveal major defects in the absence of auxin (**Fig. 5D**). In contrast, a 16h-treatment with auxin led to a ~30% decrease of both Tpr and Nup98 intensities at the nuclear envelope of neuronal progenitors compared to the control cells (**Figs. 5D** and **S4E**). This suggests a global decrease in pore number upon Seh1 depletion, comparable to the observations previously made in pluripotent *Seh1*$^{-/-}$ and *GFP-mAID-Seh1* mESCs (Gonzalez-Estevez, Verrico et al., 2021). Note that unlike Tpr and Nup98,

Nup153 levels were not altered in auxin-treated *Seh1-degron* cells, suggesting, as also observed in *Nup133Δmid* cells, an increased stoichiometry of Nup153 per NPC (**Fig. S4F**).

We also note that a 24h auxin treatment, applied to *Seh1-mAID-GFP* cells at day 2 of neuronal differentiation, was sufficient to cause a significant increase in *Nup210L* mRNA levels (**Fig. 5E**). Likewise, a 24h auxin treatment of *Nup133-degron* cells induced *Nup210L* expression (**Fig. 5E**). In contrast, 24h of auxin treatment did not led to an altered regulation of *Lhx1* in *Seh1-degron* or *Nup133-degron* cells at day 3 (**Fig. 5F**). Together, these data indicate that *Nup210L* and *Lhx1* are shared downstream targets of Nup133 and Seh1, with *Nup210L* appearing to be a gene induced early upon loss of these Y-complex Nups. On the other hand, *Lhx1* seems to need a prolonged depletion of these Y-complex Nups to become misregulated, indicating that it is likely an indirect target of Y-complex Nup-dependent regulations.

## DISCUSSION

In this study, we have shown in differentiating mESCs that a subset of genes is deregulated in the absence of Nup133. We found that neuronal progenitors lacking either Nup133 or just its middle domain share a defect in nuclear basket assembly and altered expression of *Nup210L* and *Lhx1*. While this indicates a dual function for the middle domain of Nup133, this domain is large enough (416 aa, 17 $\alpha$-helices) to possibly allow simultaneous interactions with another nucleoporin and a gene expression regulator. Alternatively, this large deletion, by shortening the length of Nup133, may also alter the head-to-tail interactions between consecutive Y-complexes, in turn affecting nuclear basket assembly or stability.

However, the basket assembly and altered gene expression phenotypes can be uncoupled. Indeed, *Nup210L* and *Lhx1* were not misregulated in our *Nup133-degron* cell lines that display a constitutive nuclear basket assembly defect, and conversely, they were both similarly misregulated in *Seh1-deficient* cells in which nuclear basket assembly is not specifically altered. As the untreated *Nup133-degron* cell lines exhibit lower Nup133 protein levels than the control cell lines, our data further argue that a limited amount of Nup133 is sufficient to keep *Nup210L* repressed in differentiating mESCs and to induce the proper and timely expression of *Lhx1*. Because this function in gene regulation is shared by Nup133 and

Seh1, two physically distant members of the Y-complex, it likely involves the whole Y-complex rather than each of these two individual subunits.

The rather short lag time (below 24h) between auxin-induced degradation of Nup133 or Seh1 and *Nup210L* activation suggests that there could be a direct contact between the Y-complex and the *Nup210L* genomic locus. Although the Y-complex is mainly visualized at NPCs to which it is stably anchored (Rabut et al., 2004), a diffuse fraction is also likely present in the nucleus, as previously described in HeLa cells (Morchoisne-Bolhy et al., 2015). Hence, Y-complex dependent gene regulation may take place either at NPCs or "off-pore". Browsing available data of LaminB1-Dam-ID tracks (Peric-Hupkes et al., 2010), we noticed that the *Nup210L* locus is adjacent to a lamin-associated domain (LAD) in mESCs and neural progenitor cells. A location near the nuclear periphery would be consistent with a regulation of *Nup210L* taking place at NPCs. In line with this hypothesis, Seh1 was shown to recruit to the NPC the transcription factor Olig2 and the chromatin remodeler Brd7 to promote the expression of differentiation genes in oligodendrocytes (Liu et al., 2019). Additionally, Nup133 was proposed to promote the expression of *Myc* in cancer cells by anchoring its superenhancer to the NPCs (Scholz et al., 2019).

This Y-complex-mediated gene regulation may also involve epigenetic mechanisms, as reported for Nup153, which interacts with PRC1 to repress developmental genes (Jacinto et al., 2015). Along these lines, it is noteworthy that human *NUP210L*, initially thought to be a testis-specific gene, was found to be expressed in prefrontal cortex neurons of some individuals. This regulation was linked to the epigenetic allele-specific activation of *NUP210L,* namely the deposition of the permissive histone mark H3K4me3 at its promoter (Gusev et al., 2019). In addition, another epigenetic mechanism, the DNA methylation state of *Nup210L,* has been linked to psychologic development disorders in patients carrying a hemizygous 22q11.2 microdeletion (Starnawska et al., 2017). Considering its possible link with normal or pathological cognitive abilities, the mechanisms of Nup133- and Seh1-dependent *Nup210L* activation warrant further investigations. It is quite remarkable that *Nup210L*, a gene encoding a nucleoporin, is one of the earliest and most robustly upregulated genes when Y-complex deficient mESCs are induced to differentiate towards neuronal fates. Although not sufficient to prevent the impaired differentiation of Nup133- and Seh1-deficient mESCs, Nup210L induction might be a tentative mechanism to compensate for improper Y-complex (and NPC) assembly in differentiating cells. Nup210L

might for example help to stabilize NPC structure or to promote NPC assembly in challenging conditions. As described for its homolog, Nup210, it may also participate in gene regulation at NPCs, or contribute via its conserved large N-terminal domain to nuclear envelope/ER homeostasis (Raices et al., 2017; Gomez-Cavazos et al., 2015). Finally, Nup210L may also indirectly impact chromatin compaction, as hypothesized in the context of impaired spermiogenesis (Arafah et al., 2021). More studies are needed to elucidate its functions in normal and pathological situations.

## MATERIALS AND METHODS

### mESCs culture and neuroectodermal differentiation

Cell lines used in this study are listed in ***Table S1*** and were grown as previously described (Gonzalez-Estevez, Verrico et al., 2021). Briefly, mESCs were grown at 37°C and 5% CO2 on Mitomycin-C inactivated feeder cells (DR4-mouse embryonic fibroblast) plated on 0.1% gelatin (Sigma-Aldrich, St Louis, MO, USA) in serum/leukemia inhibitory factor (LIF, ESGRO, Millipore, Burlington, MA, USA)-containing stem cell medium. mESCs were used at passages below 30. Lack of contamination in-between the mutant cell lines was assessed by PCR on genomic DNA, proper GFP expression when pertinent, and western blots analyses. Frequent DAPI staining ensured lack of major contamination by mycoplasms.

The neuroectodermal differentiation protocol used in this study was adapted from (Abranches et al., 2009; Ying et al., 2003), as previously described (Gonzalez-Estevez, Verrico et al., 2021). Briefly, following trypsinization and feeder removal, mESCs were resuspended in N2B27 medium [Neurobasal, DMEM-F12, 7.5% BSA, N2 supplement, B27 supplement, Pen/Strep, L-glutamin, ß-mercaptoethanol] and plated at a density of ~ $0.85x10^4$ or $3x10^4$ cells/$cm^2$ on gelatin-coated dishes (day 0). Medium was changed every day from day 2 on. To stimulate neuronal differentiation, 1µM RA (all-trans-Retinoic acid, Sigma-Aldrich) was added to the medium for 24h on day 2.

For annexin V/propidium iodide (PI) apoptosis/viability assays, cells were trypsinized, counted, and $10^5$ cells were centrifuged at 400 x *g* for 3 minutes. Cells were resuspended in 500µL of Annexin V binding buffer (ab14084, Abcam) and incubated with 1µL annexin V-Cy5 (ab14147, Abcam) and 10 µg/mL propidium iodide for 5min at room temperature in the dark. Cells were then analyzed by flow cytometry using a CyanADP Cytomation (Beckman-Coulter), using SS (side-scatter) and FS (forward scatter) to remove debris and exclude cell doublets, and 488 nm and 635 nm excitation lasers. At least 10.000 cells were acquired and data were then processed using the Summit software.

To induce degradation of the GFP-mAID-Nup133 (in *Nup133-degron* cells) and Seh1-mAID-GFP (in *Seh1-degron* cells), 500µM auxin (Sigma-Aldrich) was added to the medium (from a 280 mM stock in EtOH). The same final concentration of EtOH was added for control experiments.

**RNA-sequencing**

RNAs were extracted at days 0, 2 and 3 of differentiation from 3 independent *Nup133*$^{-/-}$ clones (KO#1, HM1-derived *Nup133*$^{-/-}$ #14; KO#2, HM1-derived *Nup133*$^{-/-}$ #19; KO#3, blastocyst-derived #319 *Nup133*$^{merm/merm}$ mESCs), and from 3 control samples (WT#1; HM1; WT#2, HM1; WT#3, blastocyst-derived #1AA *Nup133*$^{+/+}$) (See **Table S1**). Library preparation and Illumina sequencing were performed at the Ecole normale supérieure genomics core facility (Paris, France). Messenger (polyA+) RNAs were purified from 1 µg of total RNA using oligo(dT). Libraries were prepared using the strand specific RNA-Seq library preparation TruSeq Stranded mRNA kit (Illumina). Libraries were multiplexed by 9 on 2 flowcells. Two 75 bp single read sequencing runs were performed on a NextSeq 500 device (Illumina). A mean of 53.14 ± 14.72 million passing Illumina quality filter reads was obtained for each of the 18 samples.

The analyses were performed using the Eoulsan pipeline version 2.0-alpha7 (Jourdren et al., 2012), including read filtering, mapping, alignment filtering, read quantification, normalization and differential analysis: Before mapping, poly N read tails were trimmed, reads ≤40 bases were removed, and reads with quality mean ≤30 were discarded. Reads were then aligned against the *Mus musculus* genome from Ensembl version 81 using STAR (version 2.4.0k)(Dobin et al., 2013). Alignments from reads matching more than once on the reference genome were removed using Java version of samtools (Li et al., 2009). To compute gene expression, *Mus musculus* GFF genome annotation version 81 from Ensembl database was used. All overlapping regions between alignments and referenced exons were counted and aggregated by genes using the HTSeq-count algorithm (Anders et al., 2015). A first analysis revealed that one of the samples (KO#2 day2) featured an abnormally high level of ribosomal transcripts; this dataset was therefore excluded from subsequent analyses.

The rest of the analysis was carried out using the bioinformatics software R (R v4.1.2 (2021.11.01)), and open access packages, using the publicly available bioinformatics course DIYtranscriptomics.com (Berry et al., 2021). Mapped raw counts were transformed in counts per million (cpm) using the cpm function from the EdgeR package (v3.34.1). We filtered the genes that had a log2(cpm) above 1 for more than 3 samples, and then normalized their cpm using the TMM method (Robinson and Oshlack, 2010). The mean-variance relationship of the filtered normalized data was modeled by voom transformation, and a linear model was

fitted to the data using the lmfit function from the limma package (v3.48.3). Bayesian statistics for the chosen pair-wise comparisons (average KO expression compared to average WT expression for each time point) were then calculated using the eBayes function from limma, and adjusted with the BH correction. An exhaustive list of differentially expressed genes (p. value<0.05 and |log2FC|>1.5) was pulled-out using the decideTests function. Plots in **Figs. 1D and S1A** were generated in R using ggplot2 (v.3.3.5).

**Transfection and CRISPR/Cas9 genome editing**

mESCs were transfected as previously described (Souquet et al., 2018) using Lipofectamin 2000 (Invitrogen, Carlsbad, CA, USA) according to manufacturer instructions. To establish the *Nup133-Rescue, Nup133-Δmid, Nup133-degron* and *Seh1-degron* cell lines, $5{\cdot}10^5$ mESCs were co-transfected with 3µg of a plasmid directing the expression of a gRNA and high fidelity (HF) Cas9 fused to mCherry and with 3 µg of DNA sequences of interest flanked by homology directed repair arms (PCR product or linearized plasmid, see **Fig. S2**). Plasmids are listed in **Table S2**, gRNAs designed using the Benchling website (https://benchling.com) are listed in **Table S3**, and PCR primers used to generate homology-directed repair templates are listed in **Table S4**. 3 days after transfection, GFP-positive cells were FACS-sorted to select for cells expressing the tagged nucleoporin and plated on culture dishes. Individual clones were picked 6-7 days after sorting and characterized using immunofluorescence, western blot, PCR on genomic DNA and sequencing. Ploidy was assessed using chromosome spreads. Cell line characteristics are summarized in **Table S1**.

**RT-qPCR**

RNA extraction was performed using NucleoSpin RNAII isolation kit (Mascherey-Nagel) according to the manufacturer's instructions. Reverse-transcription (RT) was done with the transcriptase inverse Superscript II (Invitrogen) and random hexamers (Amersham Pharmacia), using at least 150 ng of RNA per sample. Real-time quantitative PCR was performed with SybrGreen reagents (Applied Biosystems) on a LightCycler 480 instrument (Roche Life Sciences). All mRNA level results are presented as relative to the TATA-binding protein (TBP) mRNA levels. qPCR primers used in this study are listed in supplementary **Table S5**.

**Western blots analyses**

Whole cell lysate preparations and western blot analyses were performed as previously described (Gonzalez-Estevez, Verrico et al., 2021), using 4-10% SDS-PAGE gels (Mini-Protean TGX Stain free precast gels, Bio-Rad, Hercules, CA, USA) and nitrocellulose membranes (GE healthcare). Incubations with primary antibodies were carried overnight at 4°C. Signals from HRP-conjugated secondary antibodies were detected by enhanced chemiluminescence (SuperSignal® Pico or Femto, ThermoScientific) using ChemiDoc (Bio-Rad). Antibodies used in this study are listed in ***Table S6***. The uncropped membranes are presented in **Fig. S6.**

**Immunofluorescence and quantification of nucleoporin intensity at the nuclear envelope.**

Cells grown on glass coverslips coated with 0.1% gelatin were fixed for 20 minutes in 3% paraformaldehyde (VWR, Radnor, PA) (resuspended in PBS and brought to pH 8.0 with NaOH), permeabilized 30 minutes in H-Buffer (PBS, BSA 1%, Triton 0.2%, SDS 0.02%) and incubated with the primary and secondary antibodies for 1h at room temperature in H-Buffer, with washes in H-Buffer in-between. Antibodies used in this study are listed in supplementary **Table S5**. Coverslips were then incubated 5 min with DAPI (Sigma-Aldrich, 280nM in PBS) and mounted using Vectashield (Vector, Maravai Life Sciences, San Diego, CA). Images were acquired on a DMI8 microscope (Leica Microsystems), equipped with a CSU-W1 spinning-diskhead (Yokogawa, Japan) and 2 Orca-Flash 4 V2+ sCMOS cameras (Hamamatsu), using 100x/1.4 oil objectives

Quantification of nucleoporin intensities at the nuclear envelope (NE) was performed essentially as described (Souquet et al., 2018), by mixing the cell line of interest with a reference cell line, either the *WT (OsTIR)* cell line or the *Nup133-Rescue* line, as indicated. For each field, we measured the mean intensity of 8-pixel-thick lines drawn on the nuclear rims and of a background area. After subtraction of the background, the NE intensity value obtained for each cell was normalized to the mean value obtained for the reference cells acquired in the same field. Box plots were generated using GraphPad Prism (GraphPad Software, Inc.): each box encloses 50% of the normalized values obtained, centered on the median value. The bars extend from the $5^{th}$ to $95^{th}$ percentiles. Values falling outside of this range are displayed as individual points. Statistical analyses were performed using unpaired nonparametric Mann-Whitney tests. $p<0.0001$=****, $p<0.001$=***, $p<0.01$=**, $p<0.05$=*.

**Acknowledgements:**

We are grateful to Vedrana Andric, Alessandro Berto, Marta Boira and Salomé Neuvendel for help in mESCs culture, differentiation, cell line establishment, or western blot analyses. We thank Charlène Boumendil and Pierre Therizols for helpful discussions, and Benoit Palancade, Roger Karess, Charlène Boumendil and the Doye lab members for critical reading of the manuscript. We also acknowledge the ImagoSeine core facility of the Institut Jacques Monod, member of the France BioImaging infrastructure (ANR-10-INBS-04) and GIS-IBiSA, for help with cell sorting, FACS analyses, and spinning disk imaging.

**Competing interests**

The authors declare that they have no conflict of interest.

**Funding**

Work in the laboratory of VD was supported by the Centre national de la recherche scientifique (CNRS), the "Fondation pour la Recherche Médicale" (FRM, Foundation for Medical Research) under grants No DEQ20150734355, "Equipe FRM 2015" and EQU202003010205, "Equipe FRM 2020" to VD, and by the Labex Who Am I? (ANR-11-LABX-0071; Idex ANR-11-IDEX-0005-02). CO received PhD fellowships from Ecole Doctorale BioSPC, Université Paris Cité and from the "Fondation pour la Recherche Médicale" (fourth year), AV received a post-doc grant from the Labex Who Am I? (2019 post-doc call) and B.S. was supported by ''la Fondation ARC pour la Recherche sur le Cancer'' (PDF 20130606747). The ImagoSeine core facility was supported by founds from GIS-IBISA and the France-Bioimaging (ANR-10-INBS-04) infrastructures and la Ligue contre le cancer (R03/75-79). The GenomiqueENS core facility was supported by the France Génomique national infrastructure, funded as part of the "Investissements d'Avenir" program managed by the Agence Nationale de la Recherche (contract ANR-10-INBS-0009).

**Data availability**

The RNASeq gene expression data and raw fastq files are available on the GEO repository (https://www.ncbi.nlm.nih.gov/geo/query/acc.cgi?acc=GSE218080) under accession number: GSE218080.

## AUTHOR CONTRIBUTIONS

C.O., A.V., B.S., and V.D. conceived and designed the experiments.

C.O., A.V., S.P., B.S., F.C. and S.B. performed the experiments.

C.O., A.V., S.P., L.J. and V.D. analyzed the data

C.O., A.V., and V.D. wrote the manuscript with contribution of L. J. for the method section.

## REFERENCES


**Abranches, E., Silva, M., Pradier, L., Schulz, H., Hummel, O., Henrique, D., and Bekman, E.** (2009). Neural differentiation of embryonic stem cells in vitro: A road map to neurogenesis in the embryo. *PLoS One* **4**, e6286.

**Aksenova, V., Smith, A., Lee, H., Bhat, P., Esnault, C., Chen, S., Iben, J., Kaufhold, R., Yau, K.C., Echeverria, C., et al.** (2020). Nucleoporin TPR is an integral component of the TREX-2 mRNA export pathway. *Nat. Commun.* **11**, 4577.

**Anders, S., Pyl, P.T., and Huber, W.** (2015). HTSeq-A Python framework to work with high-throughput sequencing data. *Bioinformatics* **31**, 166–169.

**Arafah K., Lopez F., Cazin C., Kherraf Z.E., Tassistro V., Loundou A., Arnoult C., Thierry-Mieg N., Bulet P., Guichaoua M.R., and Ray P.F.** (2021)**.** Defect in the nuclear pore membrane glycoprotein 210-like gene is associated with extreme uncondensed sperm nuclear chromatin and male infertility: a case report. *Hum Reprod.* **36**, 693-701.

**Berry, A.S.F., Amorim, C.F., Berry, C.L., Syrett, C.M., English, E.D., and Beiting, D.P.** (2021). An open-source toolkit to expand bioinformatics training in infectious diseases. *MBio* **12**, e0121421.

**Boumendil, C., Hari, P., Olsen, K.C.F., Acosta, J.C., and Bickmore, W.A.** (2019). Nuclear pore density controls heterochromatin reorganization during senescence. *Genes Dev.* **33**, 144–149.

**Braun, D.A., Lovric, S., Schapiro, D., Schneider, R., Marquez, J., Asif, M., Hussain, M.S., Daga, A., Widmeier, E., Rao, J., et al.** (2018). Mutations in multiple components of the nuclear pore complex cause nephrotic syndrome. *J. Clin. Invest.* **128**, 4313–4328.

**Buchwalter, A., Kaneshiro, J.M., and Hetzer, M.W.** (2019). Coaching from the sidelines: the nuclear periphery in genome regulation. *Nat. Rev. Genet.* **20**, 39–50.

**Buchwalter, A.L., Liang, Y., and Hetzer, M.W.** (2014). Nup50 is required for cell differentiation and exhibits transcription-dependent dynamics. *Mol. Biol. Cell* **25**, 2472–2484.

**Costello, I., Nowotschin, S., Sun, X., Mould, A.W., Hadjantonakis, A.K., Bikoff, E.K., and Robertson, E.J.** (2015). Lhx1 functions together with Otx2, Foxa2, and Ldb1 to govern anterior mesendoderm, node, and midline development. *Genes Dev.* **29**, 2108–2122.

**D'Angelo, M.A., Gomez-Cavazos, J.S., Mei, A., Lackner, D.H., and Hetzer, M.W.** (2012). A change in nuclear pore complex composition regulates cell differentiation. *Dev. Cell* **22**, 446–

458.

**Delay, B.D., Corkins, M.E., Hanania, H.L., Salanga, M., Deng, J.M., Sudou, N., Taira, M., Horb, M.E., and Miller, R.K**. (2018). Tissue-specific gene inactivation in xenopus laevis: Knockout of lhx1 in the kidney with CRISPR/Cas9. *Genetics* **208**, 673–686.

**Dobin, A., Davis, C.A., Schlesinger, F., Drenkow, J., Zaleski, C., Jha, S., Batut, P., Chaisson, M., and Gingeras, T.R.** (2013). STAR: Ultrafast universal RNA-seq aligner. *Bioinformatics* **29**, 15–21.

**Doucet, C.M., and Hetzer, M.W.** (2010). Nuclear pore biogenesis into an intact nuclear envelope. *Chromosoma* **119**, 469–477.

**Dultz, E., Wojtynek, M., Medalia, O., and Onischenko, E.** (2022). The Nuclear Pore Complex: Birth, Life, and Death of a Cellular Behemoth. *Cells* **11**, 1–28.

**Fujita, A., Tsukaguchi, H., and Koshimizu, E.** (2018). Homozygous Splicing Mutation in NUP133 Causes Galloway–Mowat Syndrome Atsushi. *Ann. Neurol.* **84**, 814–828.

**Gomez-Cavazos, J.S., and Hetzer, M.W.** (2015). The nucleoporin gp210/Nup210 controls muscle differentiation by regulating nuclear envelope/ER homeostasis. *J Cell Biol.* **208**, 671-81.

**Gonzalez-Estevez, A., Verrico, A., Orniacki, C., Reina-San-Martin, B., and Doye, V.** (2021). Integrity of the short arm of the nuclear pore Y-complex is required for mouse embryonic stem cell growth and differentiation. *J. Cell Sci.* **134**, jcs258340.

**Gusev, F.E., Reshetov, D.A., Mitchell, A.C., Andreeva, T. V., Dincer, A., Grigorenko, A.P., Fedonin, G., Halene, T., Aliseychik, M., Goltsov, A.Y., et al.** (2019). Epigenetic-genetic chromatin footprinting identifies novel and subject-specific genes active in prefrontal cortex neurons. *FASEB J.* **33**, 8161–8173.

**Harel, A., Orjalo, A. V., Vincent, T., Lachish-Zalait, A., Vasu, S., Shah, S., Zimmerman, E., Elbaum, M., and Forbes, D.J.** (2003). Removal of a single pore subcomplex results in vertebrate nuclei devoid of nuclear pores. *Mol. Cell* **11**, 853–864.

**Hezwani, M., and Fahrenkrog, B.** (2017). The functional versatility of the nuclear pore complex proteins. *Semin. Cell Dev. Biol.* **68**, 2–9.

**Jacinto, F. V., Benner, C., and Hetzer, M.W.** (2015). The nucleoporin Nup153 regulates embryonic stem cell pluripotency through gene silencing. *Genes Dev.* **29**, 1224–1238.

**Jourdren, L., Bernard, M., Dillies, M.A., and Le Crom, S.** (2012). Eoulsan: A cloud computing-based framework facilitating high throughput sequencing analyses. *Bioinformatics* **28**, 1542–1543.

**Jühlen, R., and Fahrenkrog, B.** (2018). Moonlighting nuclear pore proteins: tissue-specific nucleoporin function in health and disease. *Histochem. Cell Biol.* **150**, 593–605.

**Krull, S., Dörries, J., Boysen, B., Reidenbach, S., Magnius, L., Norder, H., Thyberg, J., and Cordes, V.C.** (2010). Protein Tpr is required for establishing nuclear pore-associated zones of heterochromatin exclusion. *EMBO J.* **29**, 1659–1673.

**Li, H., Handsaker, B., Wysoker, A., Fennell, T., Ruan, J., Homer, N., Marth, G., Abecasis, G.,**

**and Durbin, R.** (2009). The Sequence Alignment/Map format and SAMtools. *Bioinformatics* **25**, 2078–2079.

**Liu, Z., Yan, M., Liang, Y., Liu, M., Zhang, K., Shao, D., Jiang, R., Li, L., Wang, C., Nussenzveig, D.R., et al.** (2019). Nucleoporin Seh1 Interacts with Olig2/Brd7 to Promote Oligodendrocyte Differentiation and Myelination. *Neuron* **102**, 587–601.

**Lupu, F., Alves, A., Anderson, K., Doye, V., and Lacy, E.** (2008). Nuclear Pore Composition Regulates Neural Stem/Progenitor Cell Differentiation in the Mouse Embryo. *Dev. Cell* **14**, 831–842.

**McCloskey, A., Ibarra, A., and Hetzer, M.W.** (2018). Tpr regulates the total number of nuclear pore complexes per cell nucleus. *Genes Dev.* **32**, 1321–1331.

**McMahon, R., Sibbritt, T., Salehin, N., Osteil, P., and Tam, P.P.L.** (2019). Mechanistic insights from the LHX1-driven molecular network in building the embryonic head. *Dev. Growth Differ.* **61**, 327–336.

**Mendoza-Ochoa, G.I., Barrass, J.D., Terlouw, B.R., Maudlin, I.E., de Lucas, S., Sani, E., Aslanzadeh, V., Reid, J.A.E., and Beggs, J.D.** (2019). A fast and tuneable auxin-inducible degron for depletion of target proteins in budding yeast. *Yeast* **36**, 75–81.

**Morchoisne-Bolhy, S., Geoffroy, M.C., Bouhlel, I.B., Alves, A., Audugé, N., Baudin, X., Van Bortle, K., Powers, M.A., and Doye, V.** (2015). Intranuclear dynamics of the Nup107-160 complex. *Mol. Biol. Cell* **26**, 2343–2356.

**Ori, A., Banterle, N., Iskar, M., Andrés-Pons, A., Escher, C., Khanh Bui, H., Sparks, L., Solis-Mezarino, V., Rinner, O., Bork, P., et al.** (2013). Cell type-specific nuclear pores: A case in point for context-dependent stoichiometry of molecular machines. *Mol. Syst. Biol.* **9**, 648.

**Peric-Hupkes, D., Meuleman, W., Pagie, L., Bruggeman, S.W.M., Solovei, I., Brugman, W., Gräf, S., Flicek, P., Kerkhoven, R.M., van Lohuizen, M., et al**. (2010). Molecular Maps of the Reorganization of Genome-Nuclear Lamina Interactions during Differentiation. *Mol. Cell* **38**, 603–613.

**Rabut, G., Doye, V., and Ellenberg, J.** (2004). Mapping the dynamic organization of the nuclear pore complex inside single living cells. *Nat. Cell Biol.* **6**, 1114–1121.**Raices, M., Bukata, L., Sakuma, S., Borlido, J., Hernandez, L.S., Hart, D.O., and D'Angelo, M.A.** (2017). Nuclear pores regulate muscle development and maintenance by assembling a localized Mef2C complex. *Dev Cell.* **41**, 540-554.

**Robinson, M.D., and Oshlack, A.** (2010). A scaling normalization method for differential expression analysis of RNA-seq data. *Genome Biol.* **11**, R25.

**Scholz, B.A., Sumida, N., de Lima, C.D.M., Chachoua, I., Martino, M., Tzelepis, I., Nikoshkov, A., Zhao, H., Mehmood, R., Sifakis, E.G., et al.** (2019). WNT signaling and AHCTF1 promote oncogenic MYC expression through super-enhancer-mediated gene gating. *Nat. Genet.* **51**, 1723–1731.

**Selfridge, J., Pow, A.M., Mcwhir, J., Magin, T.M., and Melton, D.W.** (1992). Gene Targeting Using a Mouse HPRT Minigene/HPRT-Deficient Embryonic Stem Cell System: Inactivation of the Mouse ERCC-1 Gene. *Somat. Cell Mol. Genet.* **18**, 325–336.

**Shawlot, W., Wakamiya, M., Kwan, K.M., Kania, A., Jessell, T.M., and Behringer, R.R.** (1999). Lim1 is required in both primitive streak-derived tissues and visceral endoderm for head formation in the mouse. *Development* **126**, 4925–4932.

**Souquet, B., Freed, E., Berto, A., Andric, V., Audugé, N., Reina-San-Martin, B., Lacy, E., and Doye, V.** (2018). Nup133 Is Required for Proper Nuclear Pore Basket Assembly and Dynamics in Embryonic Stem Cells. *Cell Rep.* **23**, 2443–2454.

**Starnawska, A., Hansen, C.S., Sparsø, T., Mazin, W., Olsen, L., Bertalan, M., Buil, A., Bybjerg-Grauholm, J., Bækvad-Hansen, M., Hougaard, D.M., et al.** (2017). Differential DNA methylation at birth associated with mental disorder in individuals with 22q11.2 deletion syndrome. *Transl. Psychiatry* **7**, e1221.

**Subrini, J., and Turner, J.** (2021). Y chromosome functions in mammalian spermatogenesis. *eLlife* **10**, e67345

**Toda, T., Hsu, J.Y., Linker, S.B., Hu, L., Schafer, S.T., Mertens, J., Jacinto, F. V, Hetzer, M.W., and Gage, F.H.** (2017). Nup153 Interacts with Sox2 to Enable Bimodal Gene Regulation and Maintenance of Neural Progenitor Cells. *Cell Stem Cell* **21**, 618–634.

**Vollmer, B., Lorenz, M., Moreno-Andrés, D., Bodenhöfer, M., De Magistris, P., Astrinidis, S.A., Schooley, A., Flötenmeyer, M., Leptihn, S., and Antonin, W.** (2015). Nup153 Recruits the Nup107-160 Complex to the Inner Nuclear Membrane for Interphasic Nuclear Pore Complex Assembly. *Dev. Cell* **33**, 717–728.

**Walther, T.C., Alves, A., Pickersgill, H., Loïodice, I., Hetzer, M., Galy, V., Hülsmann, B.B., Köcher, T., Wilm, M., Allen, T., et al.** (2003). The conserved Nup107-160 complex is critical for nuclear pore complex assembly. *Cell* **113**, 195–206.

**Wozniak, R.W., and Blobel, G. (**1992). The single transmembrane segment of gp210 is sufficient for sorting to the pore membrane domain of the nuclear envelope. *J. Cell Biol.* **119**, 1441–1450.

**Yesbolatova, A., Saito, Y., Kitamoto, N., Makino-Itou, H., Ajima, R., Nakano, R., Nakaoka, H., Fukui, K., Gamo, K., Tominari, Y., et al**. (2020). The auxin-inducible degron 2 technology provides sharp degradation control in yeast, mammalian cells, and mice. *Nat. Commun.* **11**.

**Ying, Q.L., Stavridis, M., Griffiths, D., Li, M., and Smith, A.** (2003). Conversion of embryonic stem cells into neuroectodermal precursors in adherent monoculture. *Nat. Biotechnol.* **21**, 183–186.

**Zeng, H., Horie, K., Madisen, L., Pavlova, M.N., Gragerova, G., Rohde, A.D., Schimpf, B.A., Liang, Y., Ojala, E., Kramer, F., et al.** (2008). An inducible and reversible mouse genetic rescue system. *PLoS Genet.* **4**, e1000069.

673 **FIGURE LEGENDS**

674

675 **Figure 1. Transcriptomic analysis of *Nup133*$^{-/-}$ mESCs and early neuronal progenitors**

676 **A.** Growth curve in neuroectodermal differentiation of *WT* (HM1) and isogenic *Nup133*$^{-/-}$
677 mESCs. N2B27: neuronal differentiation medium complemented with N2 and B27
678 supplements; RA: all-trans-Retinoic acid (see Materials and Methods). The graph (logarithmic
679 scale) represents the average of cell counts from n=3 independent experiments, except for
680 day 6 (n=2), each represented by a distinct label. Values were normalized to the number of
681 cells seeded at day 0 ($3.10^4$ cells/cm$^2$). **B.** Quantification of apoptosis initiation (defined by
682 annexin V positive (+) and propidium iodide negative (PI -) cells) and cell death (propidium
683 iodide positive cells, PI+) in *WT* and *Nup133*$^{-/-}$ cells at day 3 of differentiation. Live cells
684 correspond to annexin V negative and PI negative cells. The graph represents the mean of
685 n=3 independent experiments, each represented by a distinct label. In A and B, significance
686 was assessed between *WT* and *Nup133*$^{-/-}$ using paired T. test (*p<0.05; **p<0.01). **C.** mRNA
687 levels of pluripotency (*Nanog*, *Oct4*) and neuronal progenitor (*Sox1, Pax6*) markers during
688 neuroectodermal differentiation were quantified by RT-qPCR and normalized to *Tbp* mRNA
689 levels. Each dot represents an individual experiment. The number of experiments is
690 indicated (n= ). **D.** Volcano plots of the RNA-seq analysis carried out in pluripotent mESCs
691 and in cells at day 3 of neuroectodermal differentiation, showing differentially expressed
692 genes (DEGs), by fold change (log2FC of *Nup133*$^{-/-}$ compared to *WT* cells) and significance
693 (adj. p.Val presented on a -log10 scale). The number of significantly upregulated DEGs (adj.
694 p-value<0.05, log2FC>2) and downregulated DEGs (adj. p-value<0.05, log2FC<-2) is indicated
695 at the top of each colored square. These DEGs are represented by red and blue dots,
696 respectively, if their average normalized expression in log2(CPM) is above 1. The other genes
697 are represented as black dots when their average normalized expression is above 1 and
698 otherwise as grey dots. The names of DEGs assessed by RT-qPCR (genes with adj. p-value<$10^{-2}$
699 or |log2FC|>4) are indicated in blue or red. The names of other relevant DEGs (i.e., genes
700 that fulfilled these criteria but were not assayed by qRT-PCR, namely *Krt19, Pdgfb, Cntd1,*
701 *Pik3ip1,* and *Fam196a*, and genes that belong to the same Y chromosome locus as *Eif2s3y*
702 and *Ddx3y, namely Kdm5d, Zfy1, Uba1y and Uty*) are indicated in dark grey.

703

704

**Figure 2. Altered expression of *Lhx1* and *Nup210L* in *Nup133* mutant cell lines**

**A.** Schematics of the GFP-Nup133 (*Rescue*) and GFP-Nup133Δmid fusion proteins (see also Table S1 and Fig. S2A). **B.** Western blot showing the expression of endogenous Nup133 or its GFP-tagged forms in *WT*, *Nup133*$^{-/-}$, *Nup133-Rescue* and *Nup133Δmid* cells at day 7 of differentiation. γ-tubulin is used as loading control. Molecular weights are indicated (kilodaltons). **C.** Growth curve obtained from cell counts in neuroectodermal differentiation presented in a logarithmic scale. Cells were seeded at a density of ~0.85x10$^4$ cells/cm$^2$ (3.10$^4$ cells in p12 wells). For the *Nup133Δmid* and *Rescue* cells, the lines correspond to the mean of the cell counts from the various clones (each depicted by a different symbol). The number of independent experiments for each clone is indicated (n=). n=2*: data for the *Nup133Δmid* #3 and *Rescue* #3 cell lines correspond to technical replicates (independent wells but within the same experiment). **D, E.** *Lhx1* and *Nup210L* mRNA levels were analyzed by RT-qPCR at the indicated time points of neuroectodermal differentiation in *WT (OsTIR)*, *Nup133*$^{-/-}$, *Rescue* and *Nup133Δmid* cell lines. Each cell line is represented by a distinct label. The number of biological replicates for a given cell type is indicated below each time point (n=). **F.** Left: Schematics of Nup210L and of the GFP*-mini-Nup210L construct that comprises: Nup210L predicted signal peptide (SP) and part of the luminal domain [aa 1-40], GFP* (see details about GFP* in the legend to Fig. S2) and aa 1791-1884 of Nup210L, encompassing part of its predicted luminal domain and its transmembrane TM and cytosolic (Cyt) domains. For each domain, the % of identity between mouse Nup210L and Nup210 is indicated. Numbers below the schematics correspond to amino acid residues. Right: *WT* (*HM1)* mESCs transiently expressing the GFP*-mini-Nup210L construct were fixed and processed for immunofluorescence with anti-Tpr antibodies. A single confocal section is shown. A three-fold magnification of the nuclear envelope area highlights the colocalization of GFP*-mini-Nup210L with the NPC marker Tpr within defined dots. Scale bar, 5μm.

**Figure 3. *Nup133Δmid* cells display a nuclear basket assembly defect at the neuronal progenitor stage**

**A.** Representative image (single Z-section) of Tpr and Nup153 immunofluorescence of *WT (OsTIR)* mixed with *Nup133Δmid* cells (indicated by a *) at day 5 of differentiation. Scale bar, 10μm. **B, C, D.** Quantification of Tpr (B), Nup153 (C) and Nup98 (D) fluorescence intensity at the nuclear envelope, presented as box-plots. Values were normalized to the *WT (OsTIR)* in

each field. Standard deviation (SD), number of analyzed cells (N) and of experiments (n) are indicated. ****: p-value<0.0001, n.s.: non-significant in Mann-Whitney test.

**Figure 4. Nuclear basket integrity and gene regulation are uncoupled in *Nup133-degron* cells.**

**A, B.** Western blot showing the levels of endogenous Nup133 or its GFP-mAID- (*degron*) or GFP- (*Rescue*) tagged forms in the indicated cell lines at day 5 of differentiation. In **B**, *Nup133-degron* cells at day 5 of differentiation were either treated with ethanol (used as solvent for auxin; -) or with auxin for the indicated time. 1/2 and 1/4 dilutions of the non-treated *Nup133-degron* extract were also loaded. γ-tubulin is used as loading control. Molecular weights are indicated (kilodaltons). **C.** Cell counts at day 7 of neuroectodermal differentiation (n=3). Cells were seeded at 0.85 x $10^4$ cells/$cm^2$. The graph represents the average of 3 independent experiments, each represented by a distinct label. **D.** Quantification of Tpr fluorescence intensity at the nuclear envelope in *Nup133-degron* cells treated (+) or not (-) for 16 h with auxin at day 5 of differentiation, presented as box-plots. Values were normalized to the *Nup133-Rescue* in each field. Standard deviation (SD), number of analyzed cells (N) and of experiments (n) are indicated. ****: p-value<0.0001; **: p-value<0.01; *: p-value<0.05; n.s.: non-significant in Mann-Whitney test. **E.** mRNA levels of *Lhx1* and *Nup210L* were quantified by RT-qPCR in *Nup133-degron* cells treated (dotted lines) or not (continuous lines) with auxin from day 0 on. For each cell line (represented by distinct labels) and each time point, the number of independent experiments is indicated.

**Figure 5. Seh1 depletion leads to *Lhx1* and *Nup210L* misregulation and altered NPC density in neuronal progenitors.**

**A.** Expression levels of *Lhx1* and *Nup210L* were assessed by RT-qPCR at day 3 of neuroectodermal differentiation in *WT* (HM1), *Seh1*$^{-/-}$ (#1) and *Nup133*$^{-/-}$ (#14) cells (n=3). The graph represents the average and standard deviation of 3 independent experiments, each represented by a dot. **B.** Immunofluorescence analysis of Seh1-mAID-GFP expressing cells (*Seh1-degron* #2) at day 5 of differentiation. Cells treated with EtOH or auxin for the last 16h were fixed and stained with DAPI. Scale bar, 20µm. **C.** Growth curve obtained from cell counts in neuroectodermal differentiation of *Seh1-degron* cells treated when indicated with auxin from day 2 or day 4 on. Cells were seeded at 0.85 x $10^4$ cells/$cm^2$. The line corresponds

to the mean of cell counts obtained from n=3 independent experiments, except for day 5 (n=2). **D.** Quantification of Tpr intensity at the NE at day 5 of differentiation, in the indicated cell lines. Cells were treated (+) or not (-) with auxin during the previous 16h. Values are normalized to *WT (OsTIR)* and presented as box-plots. Standard deviation (SD), number of analyzed cells (N) and of experiments (n) are indicated. ****: p-value<0.0001; n.s.: non-significant in Mann-Whitney test. **E, F**. Expression of *Lhx1* and *Nup210L* was assessed by RT-qPCR at day 3 of differentiation in cells treated with auxin (+) or EtOH (-) for the last 24 h. The number of independent experiments is indicated (n=).

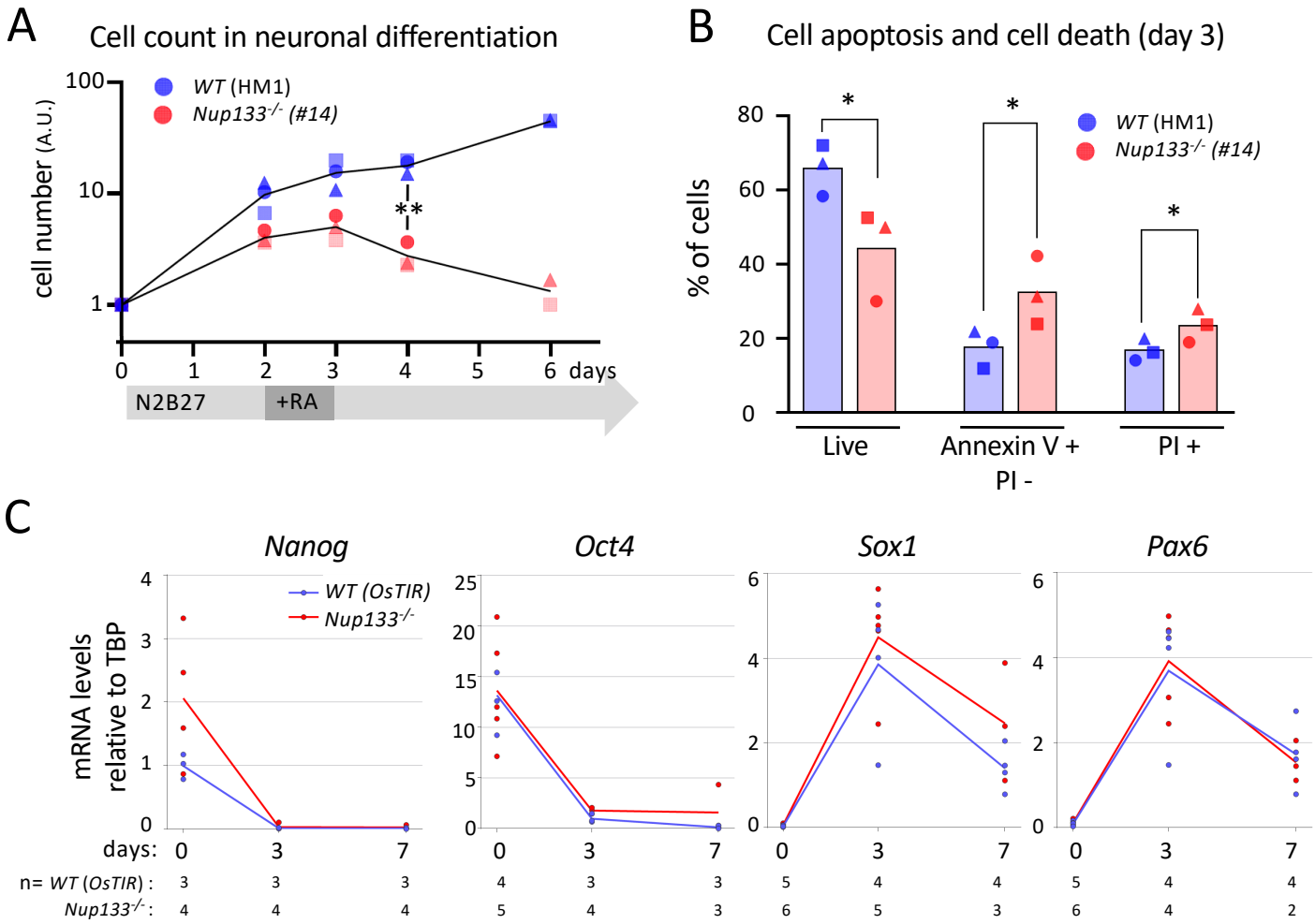


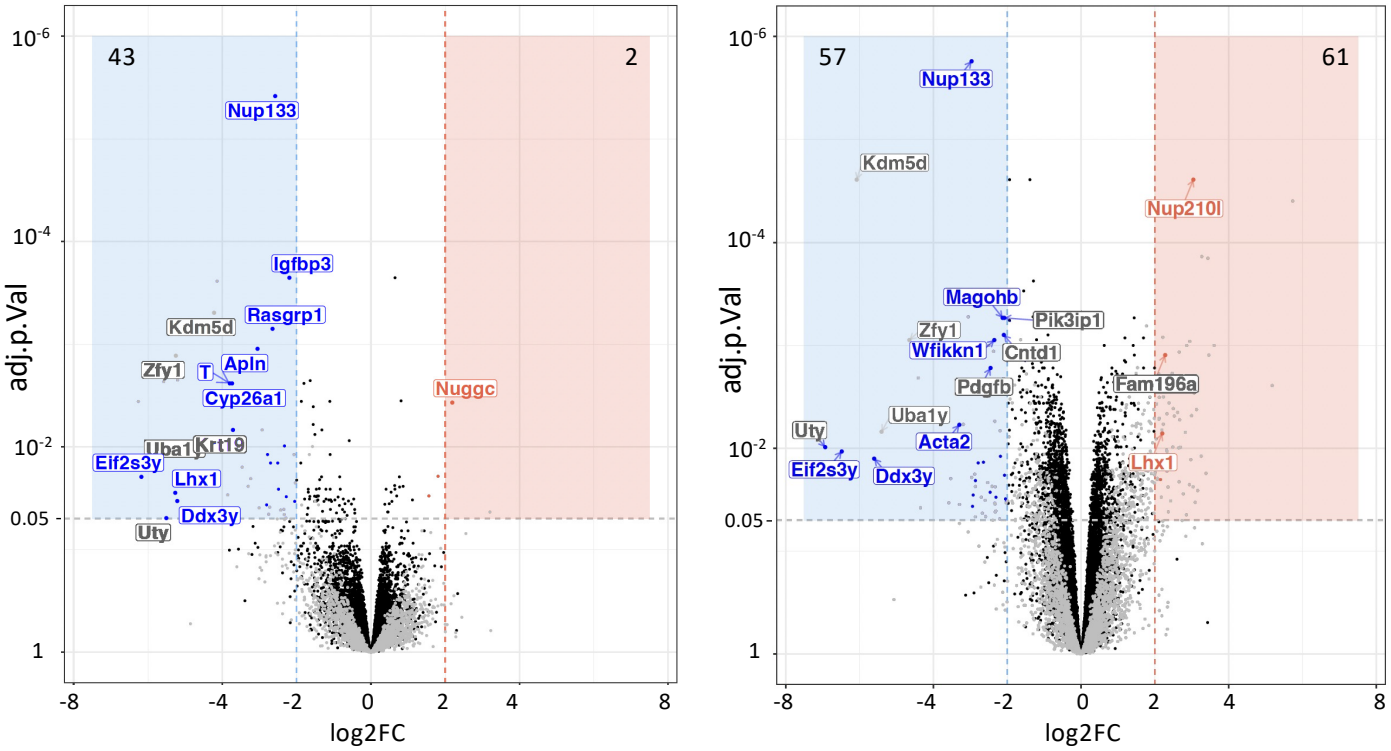


Orniacki *et al.*, Figure 1

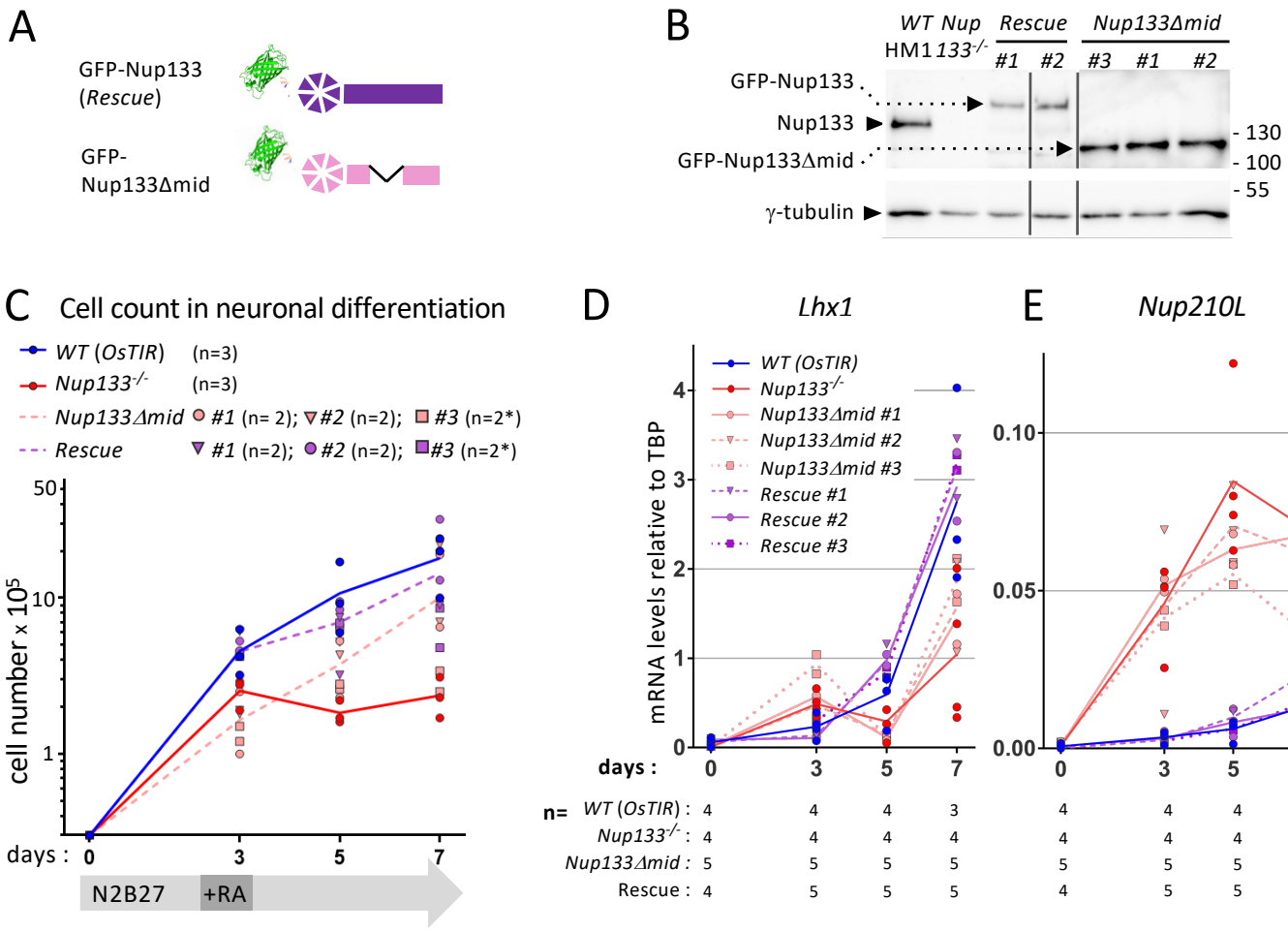


Orniacki *et al.*, Figure 2

A IF at day 5 of differentiation

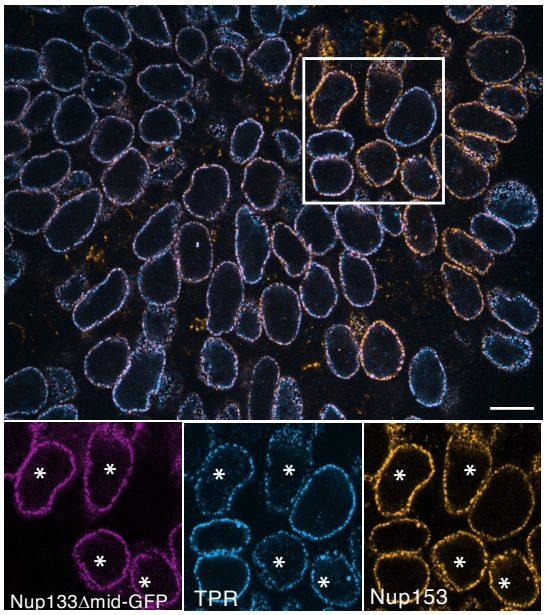


B TPR intensity at the NE (day 5)

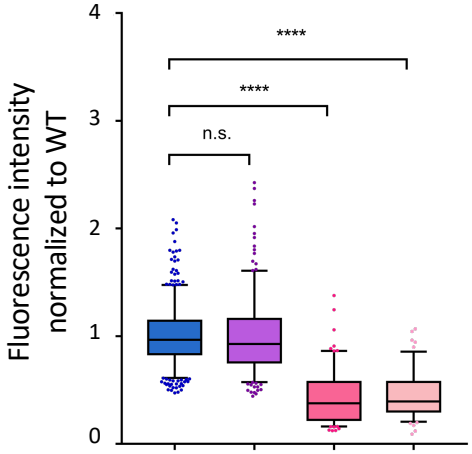


| | WT (OsTIR) | Rescue #1 | Nup133Δmid #1 | Nup133Δmid #2 |
|---|---|---|---|---|
| Mean : | 1 | 0.99 | 0.43 | 0.45 |
| ±SD : | 0.26 | 0.33 | 0.24 | 0.20 |
| N (cells) : | 546 | 297 | 145 | 117 |
| n = | 5 | 3 | 4 | 5 |

C Nup153 intensity at the NE (day 5)

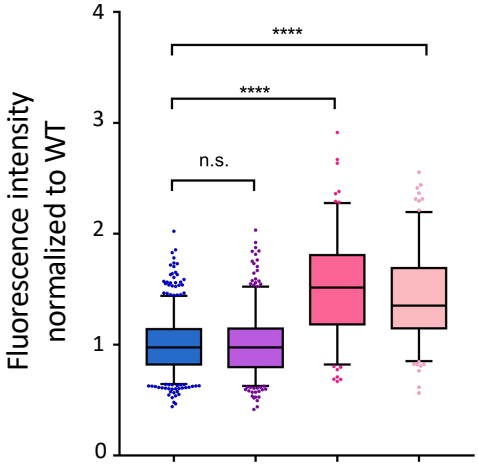


| | WT (OsTIR) | Rescue #1 | Nup133Δmid #1 | Nup133Δmid #2 |
|---|---|---|---|---|
| Mean : | 1 | 0.99 | 1.52 | 1.43 |
| ±SD : | 0.25 | 0.27 | 0.44 | 0.39 |
| N (cells) : | 648 | 414 | 152 | 165 |
| n = | 6 | 4 | 4 | 6 |

D Nup98 intensity at the NE (day 5)

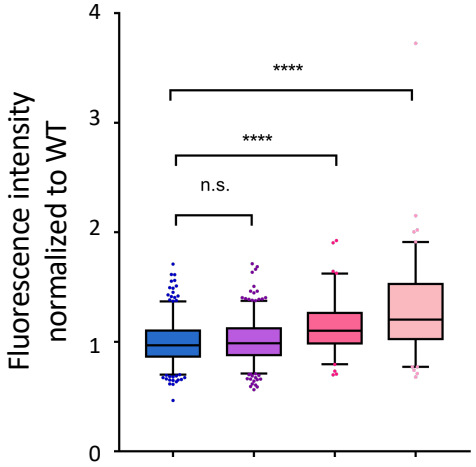


| | WT (OsTIR) | Rescue #1 | Nup133Δmid #1 | Nup133Δmid #2 |
|---|---|---|---|---|
| Mean : | 1 | 1.00 | 1.14 | 1.29 |
| ±SD : | 0.20 | 0.19 | 0.24 | 0.41 |
| N (cells) : | 263 | 337 | 90 | 102 |
| n = | 5 | 3 | 3 | 3 |

Orniacki *et al.*, Figure 3

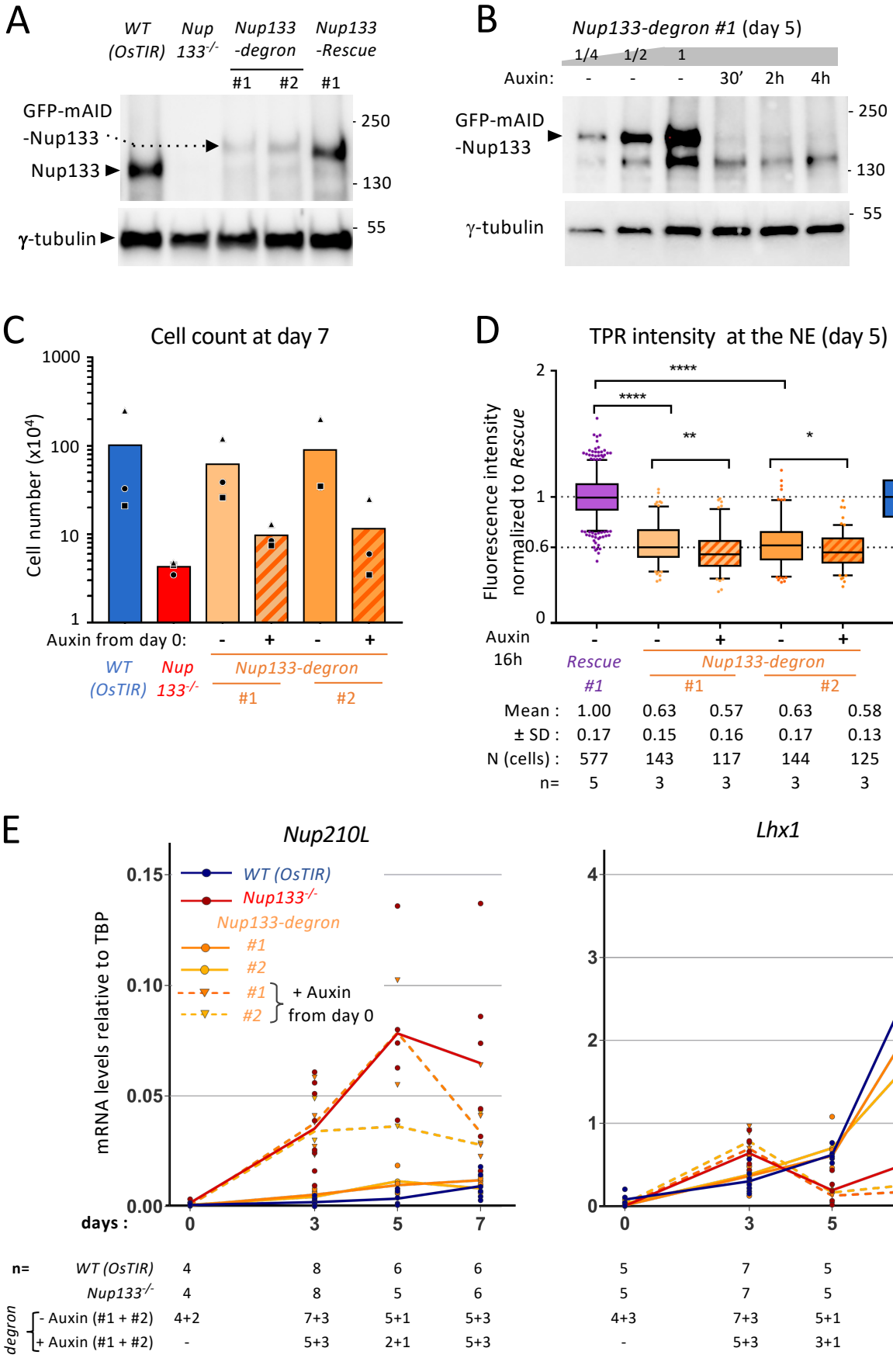


Orniacki *et al.*, Figure 4

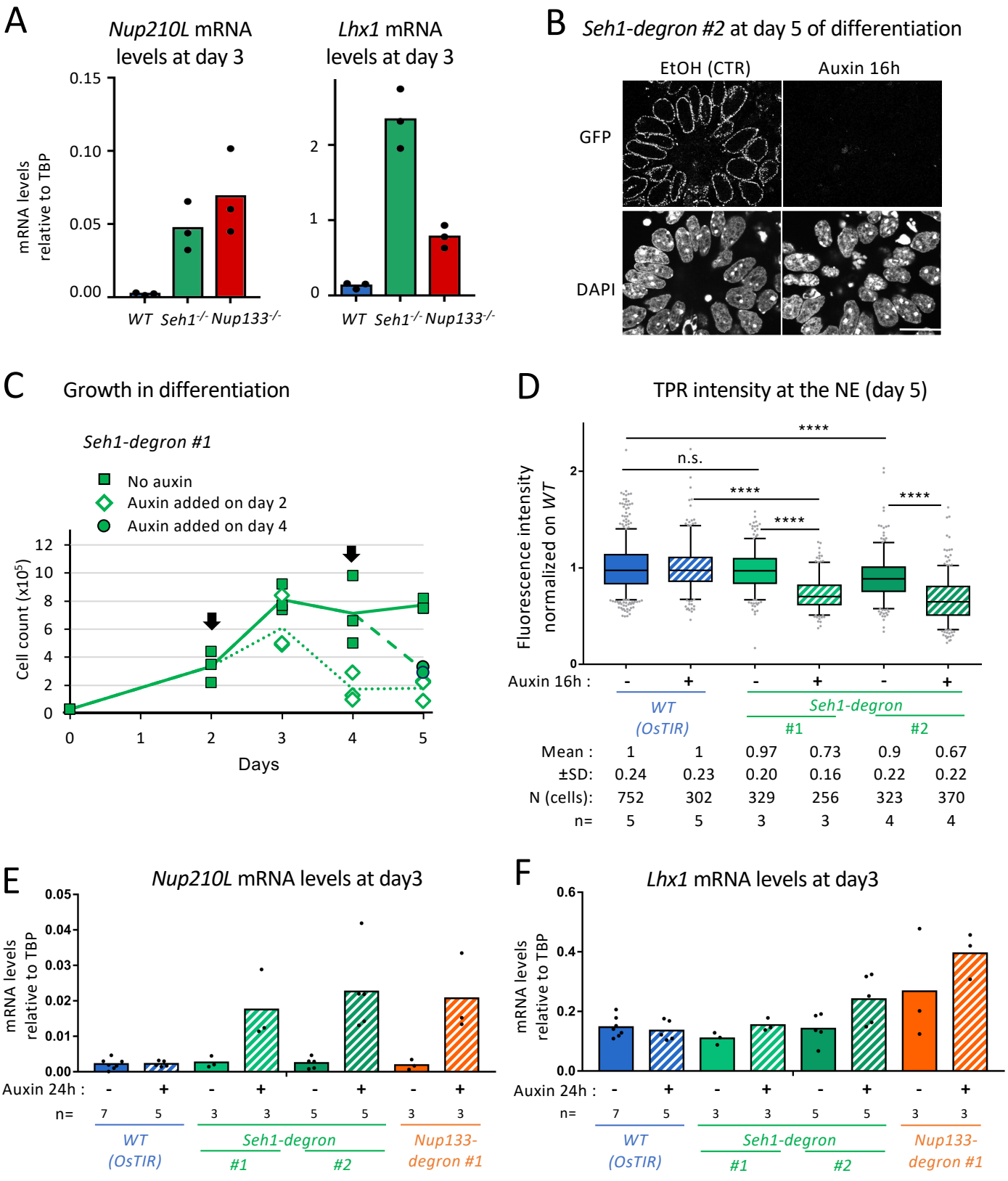


Orniacki *et al.*, Figure 5

# Inventory of Supplementary Material

**Supplemental Figures and Figure legend:**



**Supplemental Tables:**



**References cited in Supplemental Figures and Tables**

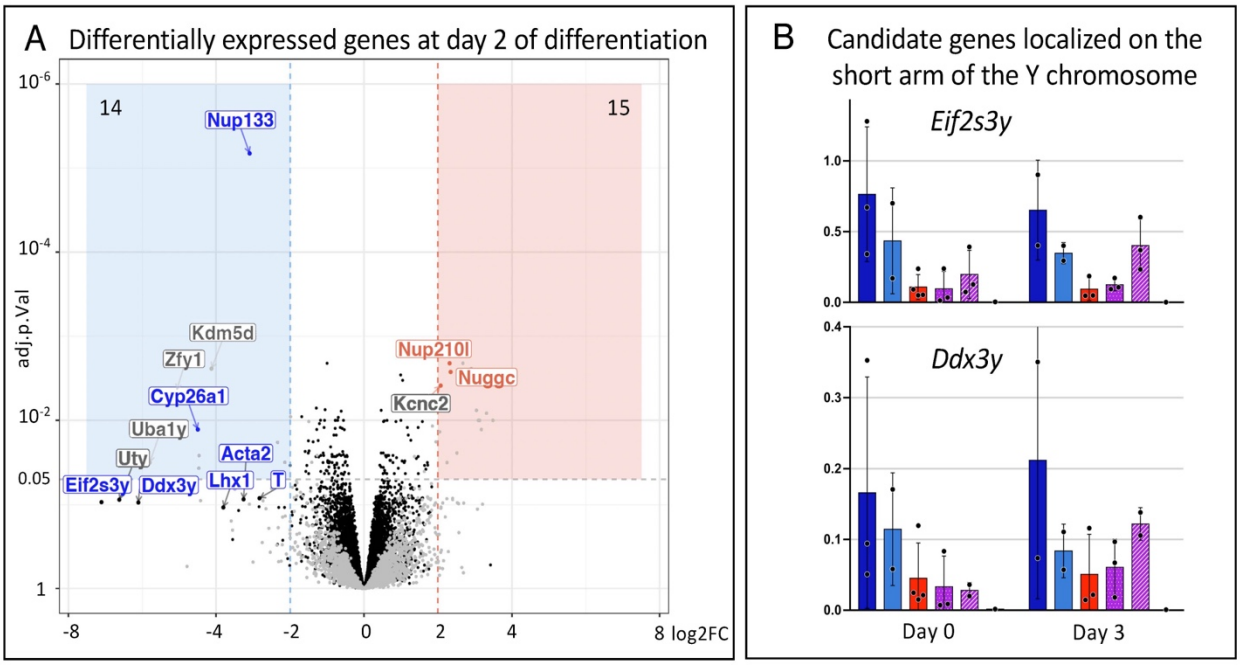
A Differentially expressed genes at day 2 of differentiation
14
15
Nup133
Kdm5d
Zfy1
Cyp26a1
Uba1y
Uty
Eif2s3y
Ddx3y
Acta2
Lhx1
T
Nup210l
Nuggc
Kcnc2
adj.p.Val
log2FC
B Candidate genes localized on the short arm of the Y chromosome
Eif2s3y
Ddx3y
Day 0
Day 3

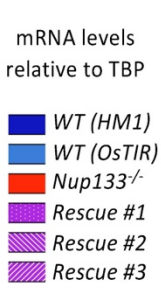
mRNA levels relative to TBP
WT (HM1)
WT (OsTIR)
Nup133-/-
Rescue #1
Rescue #2
Rescue #3

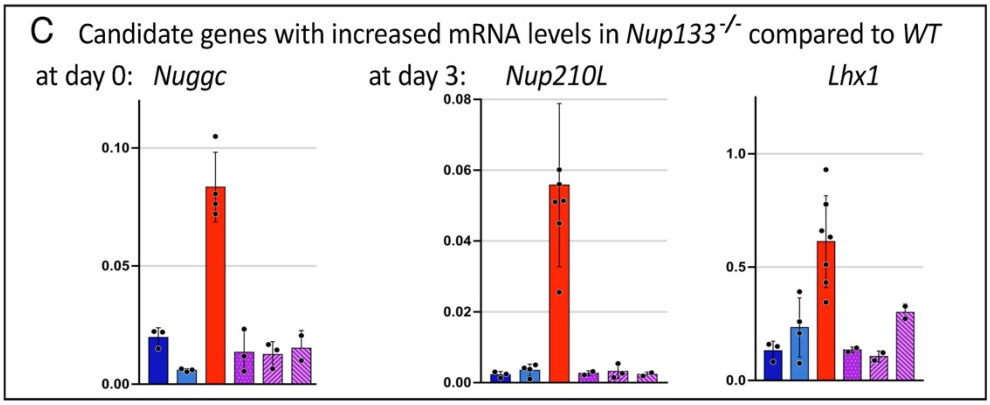
C Candidate genes with increased mRNA levels in Nup133-/- compared to WT
at day 0: Nuggc
at day 3: Nup210L
Lhx1

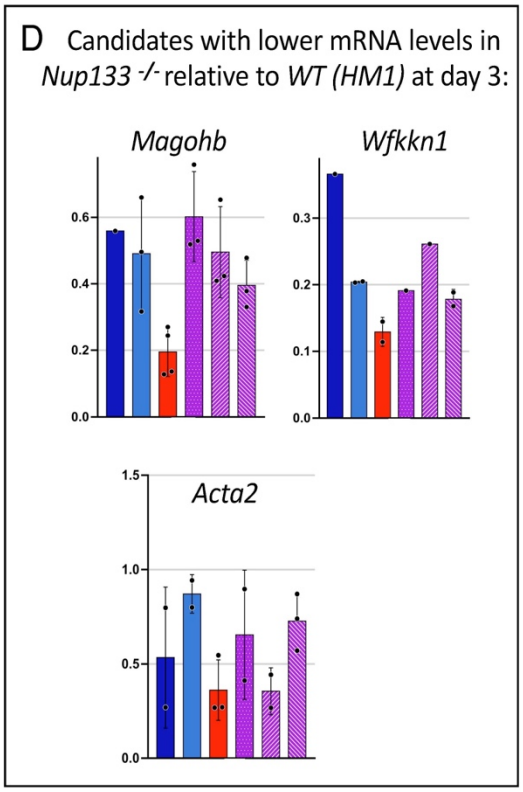
D Candidates with lower mRNA levels in Nup133 -/- relative to WT (HM1) at day 3:
Magohb
Wfkkn1
Acta2

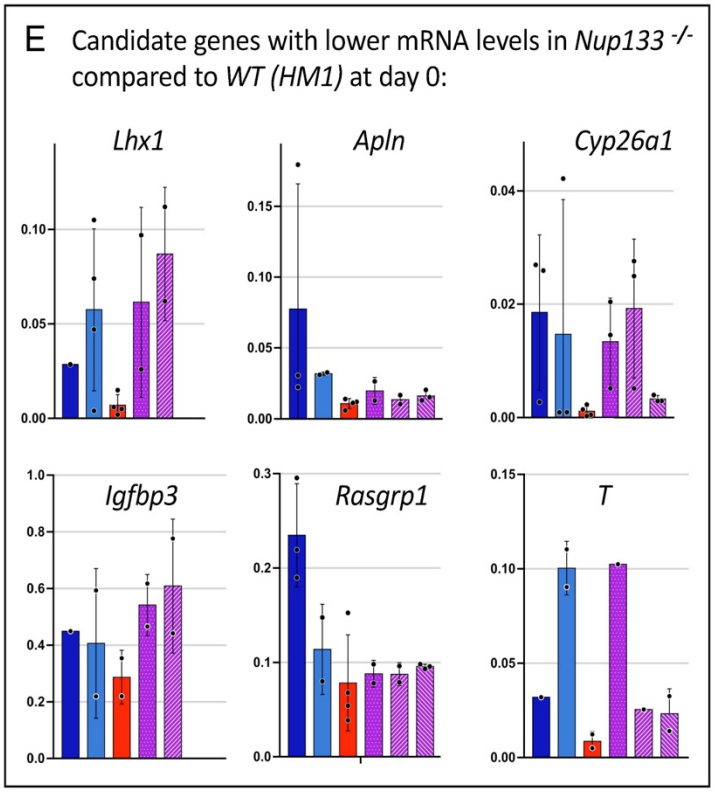
E Candidate genes with lower mRNA levels in Nup133 -/- compared to WT (HM1) at day 0:
Lhx1
Apln
Cyp26a1
Igfbp3
Rasgrp1
T

**Figure S1, related to Figure 1: DEGs analysis in differentiating *Nup133*$^{-/-}$ cells.**

**A.** Volcano plot of the RNA-seq analysis carried out in cells at day 2 of neuroectodermal differentiation, showing differentially expressed genes (DEGs), by fold change (log2FC of *Nup133*$^{-/-}$ compared to *WT*) and significance (adj. p.Val presented on a -log10 scale). The number of significantly upregulated DEGs (adj. p-value<0.05, log2FC>2) and downregulated DEGs (adj. p-value<0.05, log2FC<-2) is indicated at the top of each colored square. For this time point, the p-value of several genes is higher (less significant) due to the missing sample (see Materials and Methods). These DEGs are represented by red and blue dots, respectively, if their average normalized expression in log2(CPM) is above 1. The other genes are represented as black dots when their average normalized expression is above 1 and otherwise as grey dots. The names of DEGs assessed by RT-qPCR (genes with adj. p-value<$10^{-2}$ or |log2FC|>4) are indicated in blue or red. The names of other relevant DEGs that were not assayed by qRT-PCR (i.e., *Kcnc2*) or that are part of the same Y chromosome locus as *Eif2s3y* and *Ddx3y* are indicated in dark grey. **B-E.** mRNA levels of the indicated candidate genes (normalized to *TBP*) were measured by RT-qPCR in pluripotent mESCs or at day 3 of differentiation (see text for details). Data are presented as the mean±S.D. Each dot represents an individual experiment.

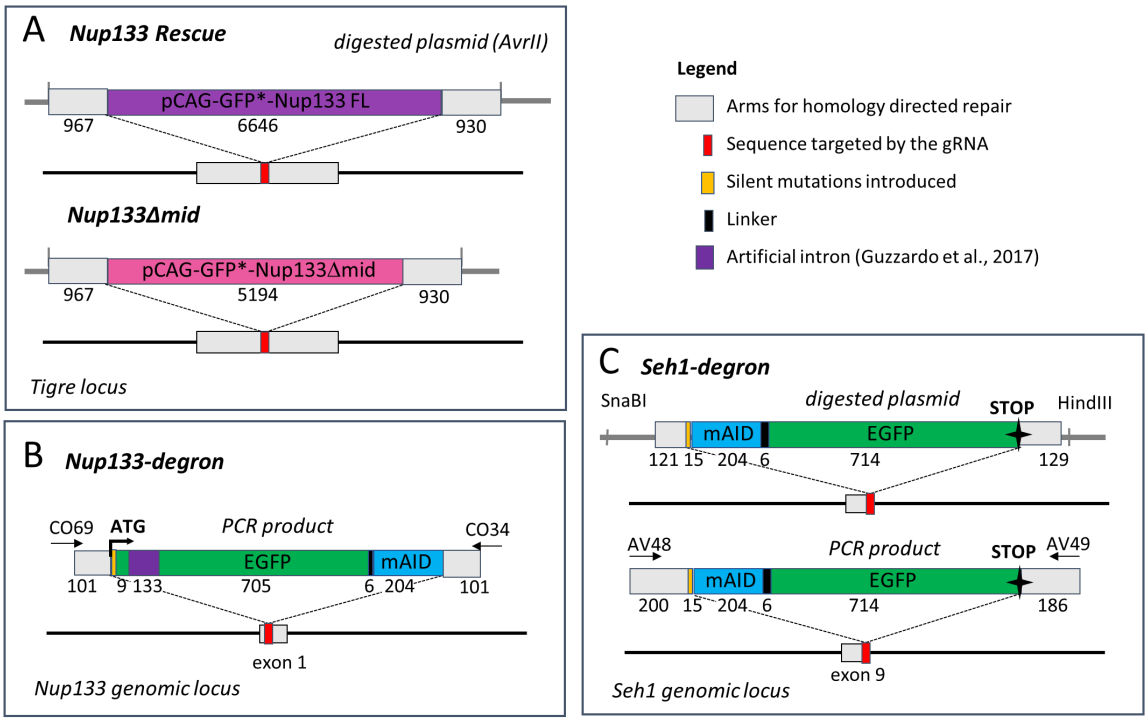


**Figure S2, related to Materials and Methods and Tables S1, S3 and S4: Schematics of CRISPR-Cas9-mediated cell line establishment via homologous recombination.** *Nup133 Rescue* and *Nup133Δmid* (**A**), *Nup133-degron* (**B**), and *Seh1-degron* **(C).** Fragment lengths are indicated in base pairs. mAID: 7kDa mini-auxin Inducible Degron (mAID) sequence (Natsume et al., 2016). Note that two different GFP-coding sequences were used in this study: GFP*, initially described in Harkins et al. (2017), contains, in addition to the S65T and F64L substitutions present in EGFP, the V163A substitution that is expected to confer it a brighter and more stable signal. In addition, the leucine introduced at position 231 during the creation of EGFP (Tsien, 1998) is reverted to the original Histidine.

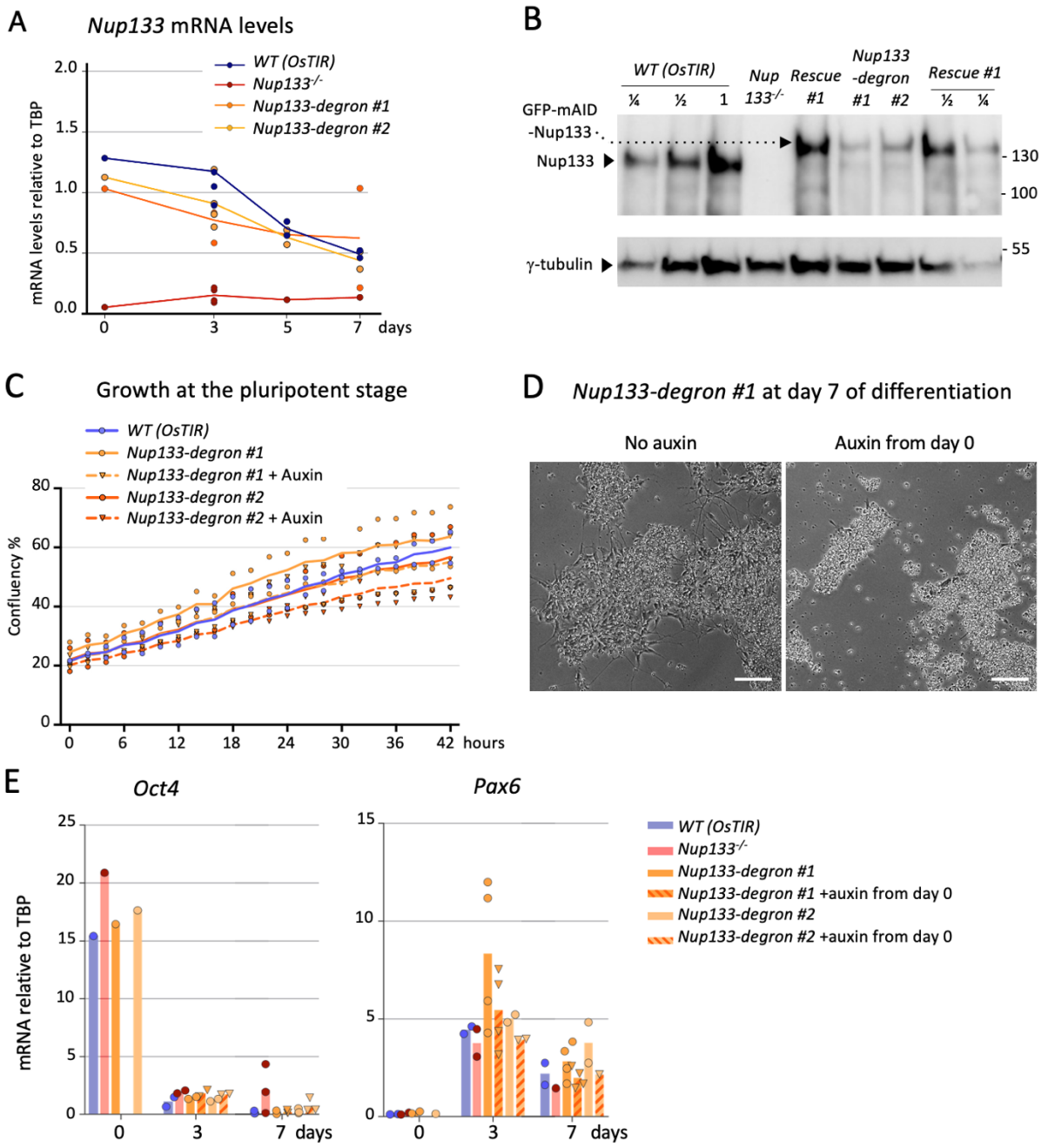


**Figure S3, related to Figure 4: Characterization of the *Nup133-degron* cell lines**.
**A.** mRNA levels of *Nup133* during differentiation, quantified by RT-qPCR and normalized to *TBP* level, are comparable in the *WT (OsTIR)* and *Nup133-degron* cell lines. **B.** Western blot showing the different expression levels of Nup133 in the *OsTIR, Nup133-degron* and *Rescue* neuronal progenitors at day 5. γ-tubulin was used as loading control. 1/2 and 1/4 dilutions of the *WT (OsTIR)* and *Rescue* extracts were also loaded. **C.** Growth of *Nup133-degron* is comparable to *WT* and not altered by addition of auxin (added at t=0) in pluripotent mESCs. Confluence values were obtained using the IncuCyte® live cell imager software (Essen Biosciences, Ann Arbor, MI) as previously described (Gonzalez-Estevez, Verrico et al., 2021). The graph corresponds to the mean of n= 2 independent experiments. **D.** Images of *Nup133-degron* cells, treated or not with auxin from day 0, were acquired at day 7 of differentiation using a widefield microscope. Neuronal rosettes and axons are visible in untreated cells while major cell death is observed in auxin-treated *Nup133-degron* cells. Scale bars, 100µm. **E.** RT-qPCR analyses show that auxin-treated *Nup133-degron* cells properly repress the pluripotency marker *Oct4* and induce the neuronal progenitor marker *Pax6* when induced to differentiate towards neuroectoderm. Each dot corresponds to an individual experiment.

A TPR intensity at the NE (pluripotent)

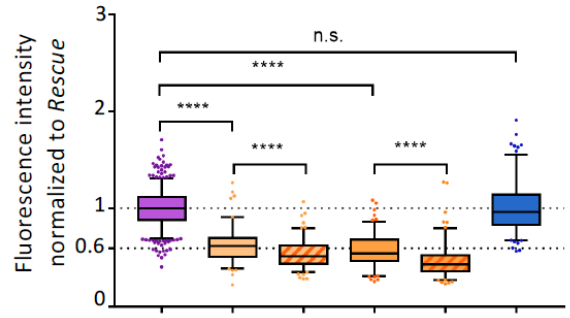


| Auxin 24h : | - | - | + | - | + | - |
|---|---|---|---|---|---|---|
| | *Rescue* | *Nup133-degron* | | | | *WT* |
| | *#1* | *#1* | | *#2* | | *(OsTIR)* |
| Mean : | 1.00 | 0.63 | 0.54 | 0.57 | 0.47 | 1.01 |
| ±SD : | 0.19 | 0.17 | 0.14 | 0.16 | 0.17 | 0.25 |
| N (cells) : | 555 | 119 | 128 | 135 | 121 | 156 |
| n = | 5 | 3 | 3 | 3 | 3 | 4 |

B Nup153 intensity at the NE (pluripotent)

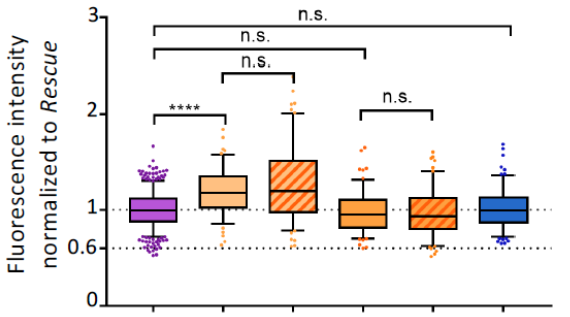


| Auxin 24h : | - | - | + | - | + | - |
|---|---|---|---|---|---|---|
| | *Rescue* | *Nup133-degron* | | | | *WT* |
| | *#1* | *#1* | | *#2* | | *(OsTIR)* |
| Mean : | 1.00 | 1.19 | 1.27 | 0.97 | 0.97 | 1.01 |
| ±SD : | 0.18 | 0.24 | 0.37 | 0.21 | 0.23 | 0.20 |
| N (cells) : | 560 | 119 | 128 | 135 | 121 | 156 |
| n = | 5 | 3 | 3 | 3 | 3 | 4 |

C Nup98 intensity at the NE (day 5)

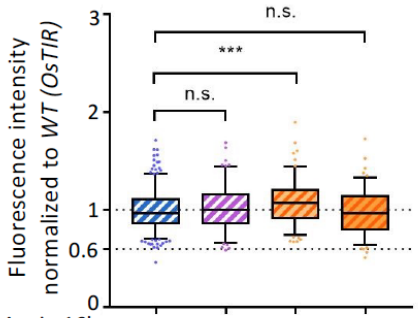


| Auxin 16h : | + | + | + | + |
|---|---|---|---|---|
| | *WT* | *Rescue* | *Nup133-degron* | |
| | *(OsTIR)* | *#1* | *#1* | *#2* |
| Mean : | 1.00 | 1.02 | 1.07 | 0.97 |
| ±SD : | 0.20 | 0.23 | 0.22 | 0.22 |
| N (cells) : | 322 | 120 | 132 | 119 |
| n = | 5 | 3 | 3 | 3 |

D Nup153 intensity at the NE (day 5)

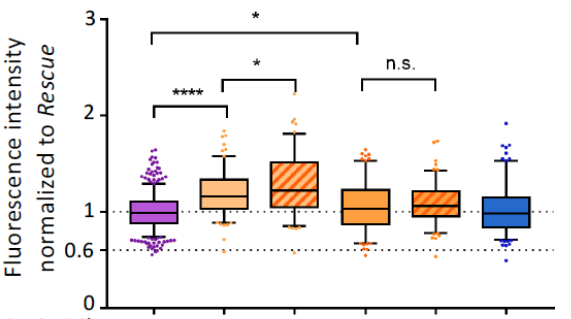


| Auxin 16h : | - | - | + | - | + | - |
|---|---|---|---|---|---|---|
| | *Rescue* | *Nup133-degron* | | | | *WT* |
| | *#1* | *#1* | | *#2* | | *(OsTIR)* |
| Mean : | 1.00 | 1.19 | 1.28 | 1.06 | 1.08 | 1.01 |
| ±SD : | 0.18 | 0.22 | 0.30 | 0.24 | 0.20 | 0.24 |
| N (cells) : | 577 | 143 | 117 | 144 | 125 | 173 |
| n = | 5 | 3 | 3 | 3 | 3 | 4 |

E Nup98 intensity at the NE (day 5)

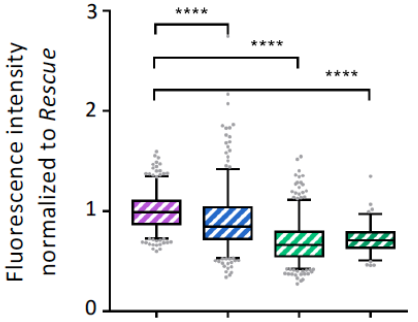


| Auxin 16h : | + | + | + | + |
|---|---|---|---|---|
| | *Rescue* | *WT* | *Seh1-degron* | |
| | *#1* | *(OsTIR)* | *#1* | *#2* |
| Mean : | 1.00 | 0.90 | 0.69 | 0.71 |
| ±SD : | 0.18 | 0.30 | 0.21 | 0.14 |
| N (cells) : | 340 | 368 | 411 | 98 |
| n = | 3 | 3 | 3 | 1 |

F Nup153 intensity at the NE (day 5)

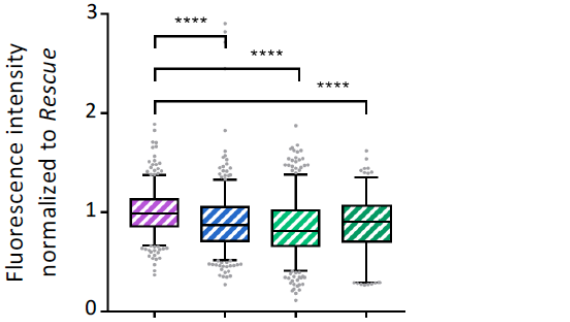


| Auxin 16h : | + | + | + | + |
|---|---|---|---|---|
| | *Rescue* | *WT* | *Seh1-degron* | |
| | *#1* | *(OsTIR)* | *#1* | *#2* |
| Mean : | 1.00 | 0.91 | 0,84 | 0,86 |
| ±SD : | 0.22 | 0.32 | 0.28 | 0.31 |
| N (cells) : | 419 | 459 | 470 | 175 |
| n = | 3 | 3 | 3 | 2 |

**Figure S4, related to Figure 3, B-D and Figure 4D: Nucleoporin densities at the nuclear envelope in *Nup133-degron* and *Seh1-degron* cell lines.**
Fluorescence intensity at the nuclear envelope of Tpr (**A**), Nup153 (**B, D, F**) and Nup98 (**C, E**) was quantified in *Nup133-degron* cells at the pluripotent stage (**A, B**), in *Nup133-degron* cells at day 5 of differentiation (**C, D**), and in *Seh1-degron* cells at day 5 of differentiation (**E, F**) and is presented as box-plots. Cells were treated with auxin (+) or ethanol (-) as control for 24 h or 16h as indicated. Values were normalized in each field to the *Nup133-Rescue* (**A, B, D, E, F**) or *WT (OsTIR*) cells (**C**) and are presented as box-plots. Standard deviation (SD), number of analyzed cells (N) and of experiments (n) are indicated. ****: p-value<0.0001; ***: p-value<0.001; **: p-value<0.01; *: p-value<0.05; n.s.: non-significant in Mann-Whitney test. Note that Nup153 levels at the NE are mildly affected in a similar manner in pluripotent and differentiated *Nup133-degron* cell lines, with a mild increase observed mainly in *Nup133-degron #1* cells treated or not with auxin (compare panels B and D). In contrast, Tpr levels are strongly decreased in both cell lines (compare panel B with Figure 1E). Note also that in auxin-treated *Seh1-degron* cells, the decreased NE level of Nup98 (panel **E**) (and of Tpr, see Figure 3D) but not of Nup153 (panel F) is consistent with a decreased NPC density combined with an increased stoichiometry of Nup153 per NPC.

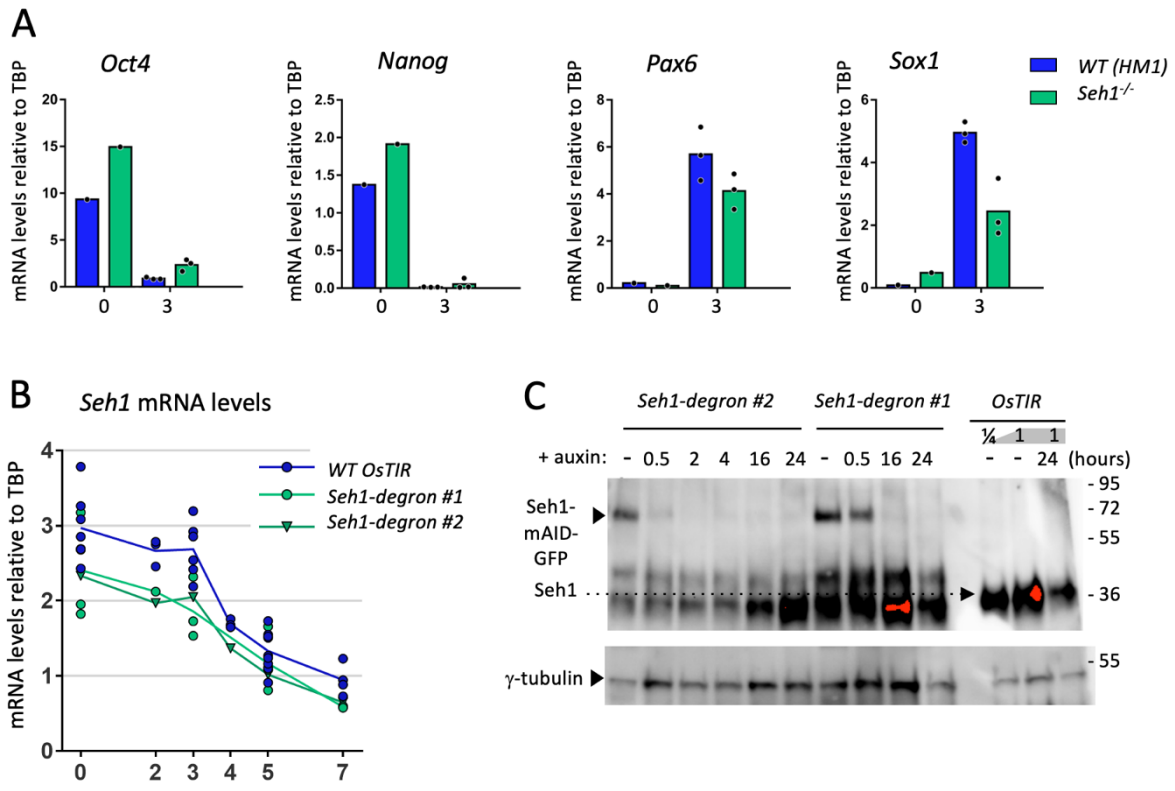


**Figure S5, related to Figure 5: Characterization of the *Seh1*$^{-/-}$ *and Seh1-degron* cell lines**
**A.** mRNA levels of pluripotency (*Oct4*, *Nanog*) and neuronal progenitor (*Pax6*, *Sox1*) markers were analyzed by RT-qPCR in *WT (HM1)* and *Seh1*$^{-/-}$ mESCs at the pluripotent stage (n=1) and after 3 days of neuroectodermal differentiation (n=3). **B.** *Seh1* mRNA levels during differentiation, quantified by RT-qPCR and normalized to *TBP* level, are comparable in the *WT (OsTIR)* and the two *Seh1-degron* cell lines (#1 and #2). Each dot corresponds to an individual experiment. **C.** Western blot showing Seh1 levels upon auxin treatment in cells at day 5 of differentiation. The membrane was first hybridized with the Seh1 antibody, then stripped to perform γ-tubulin hybridization.

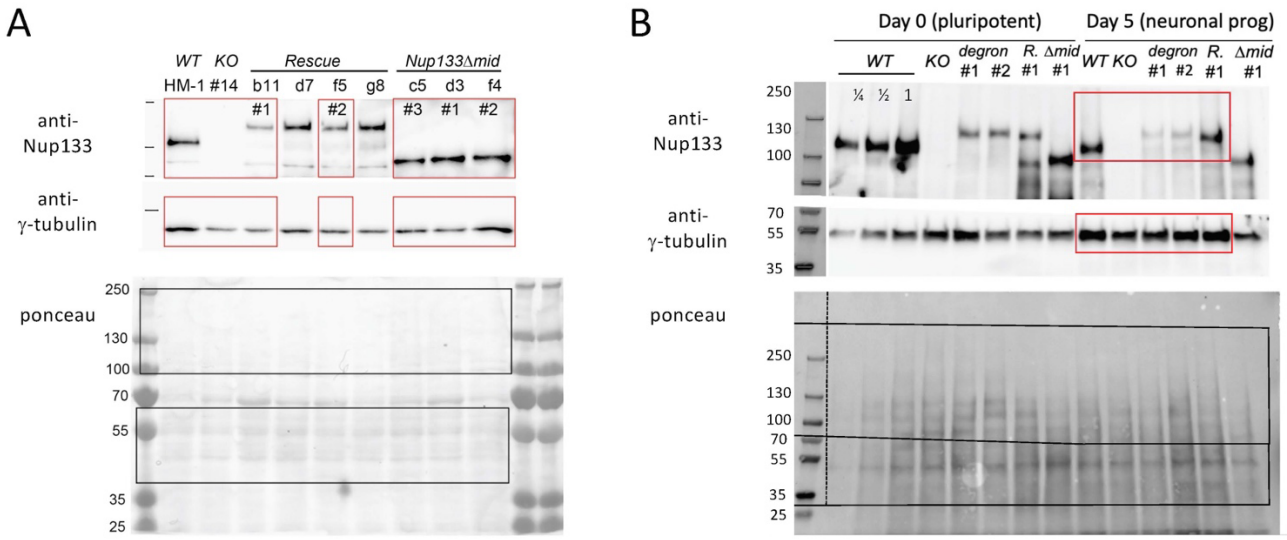
A
WT KO Rescue Nup133Δmid
HM-1 #14 b11 d7 f5 g8 c5 d3 f4
#1 #2 #3 #1 #2
anti-Nup133
anti-γ-tubulin
ponceau
250 130 100 70 55 35 25
B
Day 0 (pluripotent) Day 5 (neuronal prog)
WT KO degron #1 #2 R. #1 Δmid #1 WT KO degron #1 #2 R. #1 Δmid #1
¼ ½ 1
anti-Nup133
anti-γ-tubulin
ponceau
250 130 100 70 55 35 25

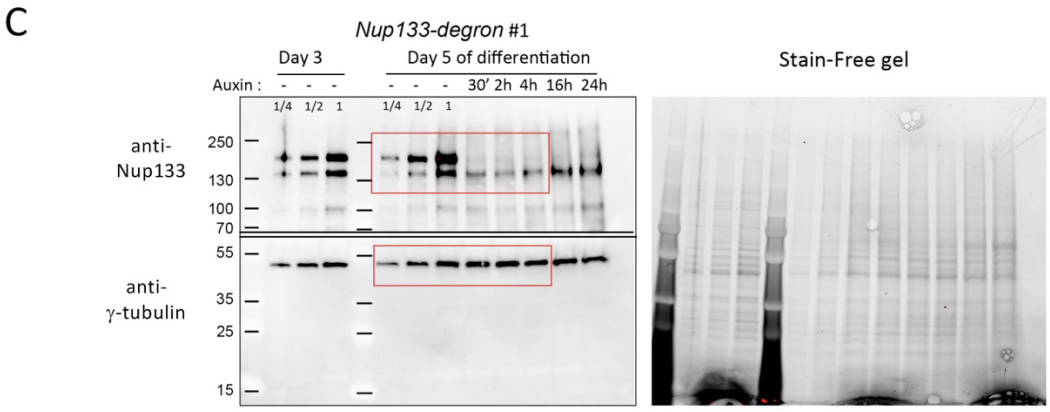
C
Nup133-degron #1
Day 3 Day 5 of differentiation
Auxin : - - - - - - 30' 2h 4h 16h 24h
1/4 1/2 1 1/4 1/2 1
anti-Nup133
anti-γ-tubulin
250 130 100 70 55 35 25 15
Stain-Free gel

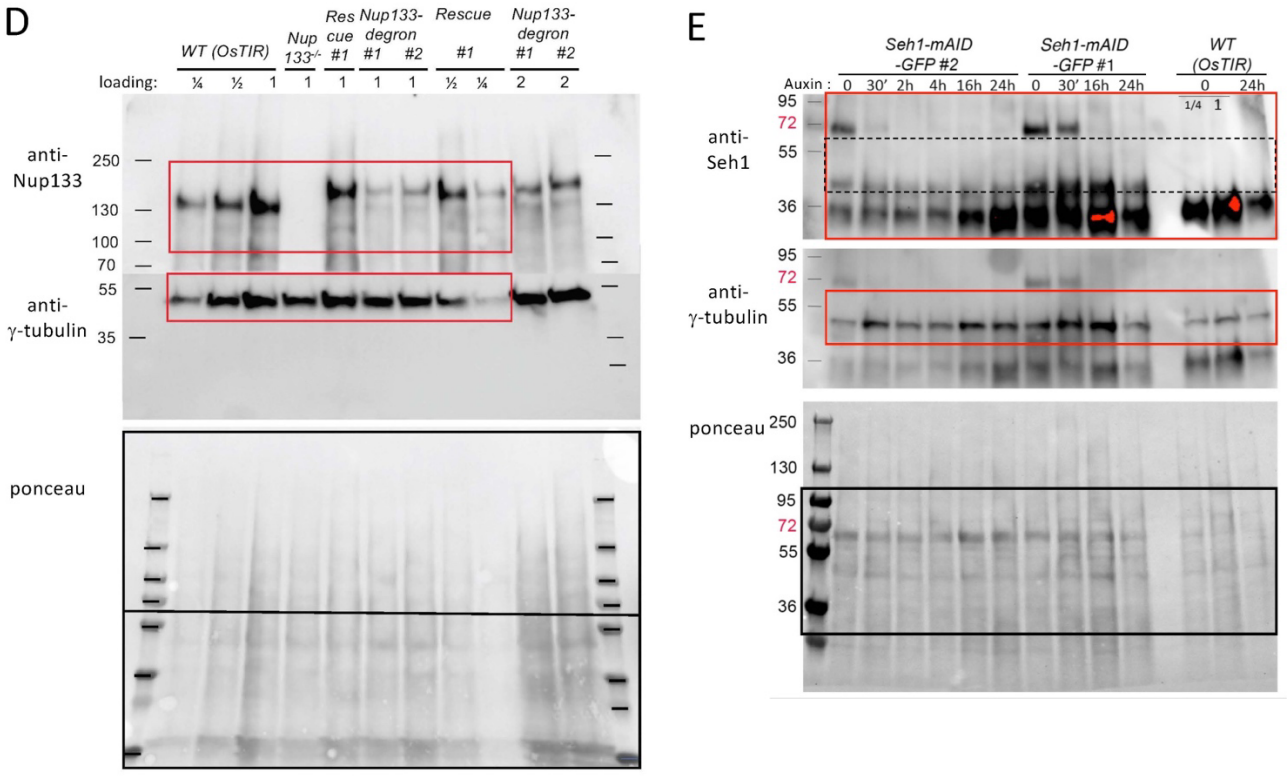
D
WT (OsTIR) Nup 133-/- Rescue #1 Nup133-degron #1 #2 Rescue #1 Nup133-degron #1 #2
loading: ¼ ½ 1 1 1 1 1 ½ ¼ 2 2
anti-Nup133
anti-γ-tubulin
ponceau
250 130 100 70 55 35
E
Seh1-mAID -GFP #2 Seh1-mAID -GFP #1 WT (OsTIR)
Auxin : 0 30' 2h 4h 16h 24h 0 30' 16h 24h 0 24h
1/4 1
anti-Seh1
anti-γ-tubulin
ponceau
95 72 55 36 250 130

**Figure S6, related to Materials and Methods: Entire gels used for western blot Figures**
Images of total protein levels, visualized either by ponceau staining of the nitrocellulose membrane or by the Stain-free staining of the TGX-gel (Bio-Rad) before transfer are also presented. The black rectangles on the nitrocellulose membranes correspond to the areas of the gels that were incubated with the indicated antibodies. Red rectangles correspond to the areas presented in the final figures.
**A, related to Fig. 2B.** *Rescue* clones b11 and f5 were renamed #1, and #2 respectively and *Nup133ΔMid* clones c5 and d3 and f4 were renamed #3, #1, and #2 respectively. Unlike the clones used in Fig. 2B, the "*Rescue"* lines d7 and g8 had the pCAG-GFP-Nup133 transgene inserted at both *Tigre* loci and were therefore not used in this study. **B, C, related to Figs. 4A,B**, were used to characterize the *Nup133-degron* cell lines in neuronal progenitors. **D, related to Fig. S3**, was used to characterize the *Nup133-degron* cell lines in pluripotent mESCs. **E, related to Fig. S5,** was used to characterize the *Seh1-degron* cell lines at day 5 of differentiation. Note that the membrane was successively probed with the anti-Seh1 and anti-γ-tubulin antibodies, explaining the residual labelling in the anti-γ-tubulin panel. The black dotted box on the anti-Seh1 gel points to the area used to detect γ-tubulin.

**Table S1, related to Experimental Procedures: Cell lines used in this study**

| NAME | SOURCE (IF PUBLISHED OR COMMERCIAL) OR DESIGN FOR CELL LINES GENERATED IN THIS STUDY | IDENTIFIER | Plate ref. | MUTATIONS (genomic sequences set at 1 for the first ATG) | Chromosome count/ Karyotype |
|---|---|---|---|---|---|
| **MEF (DR4)** | Applied StemCell | ASF-1001 | - | - | - |
| ***WT* (1A4)** | LACY lab (Souquet et al, 2018) | #1A4 | - | *Sox1*$^{gfp/+}$ | 40 Chr (68%) (XY) |
| ***merm #319*** | LACY lab (Souquet et al, 2018) | #319 | - | *Nup133*$^{merm/merm}$; *Sox1*$^{gfp/+}$ | 42 Chr XX, +8, +12 |
| ***WT* mESCs (HM1)** | ThermoFisher Scientific (Selfridge et al., 1992) | MES4303 | - | - | 40 Chr (XY) |
| ***Nup133*** $^{-/-}$ | DOYE lab - Generated by CRISPR/Cas9 editing. #14 was described in (Souquet et al., 2018); #19 is a distinct clone that arose from the same editing<br>Parental cell line: HM1<br>Cas9 & gRNA plasmids:<br>pX-102: (two tru gRNAs flanking Nup133 exon 2 andCas9-mCherry)<br>AND pX-98: two gRNAs within mNup133 exon 6 and nCas9-EGFP | *Nup133*$^{-/-}$ (#14) | #14 | Allele 1: 35 bp deletion in exon 6 (Δ11094-111128), leading to a frameshift after aa 259.<br>Allele 2: large deletion encompassing exons 2-6 (Δ2525-11143) causing a frameshift after aa 59.<br>Very low mRNA levels due to premature stop codons. No protein detected by western blot. | 40 Chr |
| | | *Nup133*$^{-/-}$ (#19) | #19 | Allele 1: 34 bp deletion in exon 6 (Δ11095-11128), leading to a frameshift after aa 260.<br>Allele 2: deletions removing (i) part of exon 2 including its 5' splice site (Δ2539-2719) and (ii) exon 3- 6 (Δ4075-11094). Expected to cause a frameshift after aa 59.<br>Very low mRNA levels due to premature stop codons. No protein detected by western blot. | ND |
| ***Seh1*** $^{-/-}$ | DOYE lab (Gonzalez-Estevez, Verrico *et al*, 2021) | *Seh1*$^{-/-}$ #1 | A18 | As described in (Gonzalez-Estevez, Verrico *et al*, 2021). | 40 Chr (>60%) |
| ***Nup133 Rescue*** | Parental cell line: *Nup133*$^{-/-}$ (#14)<br>Cas9 & gRNA plasmid: pU6-sgTIGRE_CBh-Cas9-T2A-mCherry-3UTR (#2061)<br>HR template: linearized (with AvrII) pTIGRE-CAG-GFP*mNup133FL (#2103) | *Nup133-Rescue #1* | B11 | Insertion of pCAG-GFP*-Nup133 in one of the *Tigre* alleles | ND |
| | | *Nup133-Rescue #2* | F5 | Insertion of pCAG-GFP*-Nup133 in one of the *Tigre* alleles | 41 Chr (40%)<br>40 Chr (33%)<br>42 Chr (23%) |
| | | *Nup133-Rescue #3* | G5 | Insertion of pCAG-GFP*-Nup133 in one of the *Tigre* alleles | ND |

| | | | | | |
|---|---|---|---|---|---|
| ***Nup133-Δmid*** | Parental cell line: *Nup133*$^{-/-}$ (#14)<br>Cas9 & gRNA plasmid: pU6-sgTIGRE_CBh-Cas9-T2A-mCherry-3UTR (#2061)<br>HR template: linearized (with AvrII) pTIGRE-CAG-GFP*mNup133dMid (#2102) | *Nup133-Δmid #1* | D3 | Insertion of pCAG-GFP*-Nup133Dmid in one of the *Tigre* alleles | 40 Chr (71%) |
| | | *Nup133-Δmid #2* | F4 | Insertion of pCAG-GFP*-Nup133Dmid in one of the *Tigre* alleles | 40 Chr (70%) |
| | | *Nup133-Δmid #3* | C5 | Insertion of pCAG-GFP*-Nup133Dmid in one of the *Tigre* alleles | 40 (73%) |
| ***WT (OsTIR)*** | As described in (Gonzalez-Estevez, Verrico *et al*, 2021), but a distinct clone<br>Parental cell line: HM1<br>Cas9 & gRNA plasmid: pU6-sgTIGRE_CBh-Cas9-T2A-mCherry-3UTR (#2061)<br>HR template: linearized (with EcoRV) TIGRE HR-pCAG-OsTir-T2A-NeoR-TIGRE HR (#2064) | *OsTIR* | 5F | Insertion of pCAG-OsTir-T2A-NeoR in one of the *Tigre* alleles. | 40 Chr |
| ***Nup133-degron (GFP-mAID-Nup133)*** | Parental cell line: *OsTIR (5F)*<br>Cas9 & gRNA plasmid: Cas9HF-Cherry-1gRNA-degron-Nup133<br>HR template: PCR product: HR-EGFP-mAID-mNup133 (gRNA resistant)-HR; amplification of plasmid #2108 with primers CO69-CO34 | *Nup133-degron #1* | B7 | Allele 1: insertion of EGFP-mAID after the ATG of Nup133<br>Allele 2: 10bp deletion at +1 | 40 (100%) |
| | | *Nup133-degron #2* | C8 | Allele 1: insertion of EGFP-mAID after the ATG of Nup133<br>Allele 2: 1bp insertion at +10 | 40 (74%) |
| ***Seh1-degron (Seh1-mAID-GFP)*** | Parental cell line: *OsTIR (5F)*<br>Cas9 & gRNA plasmid: **#2115_**Cas9mCherry_gRNA-Seh1Cterm<br>gRNA sequence: AGCTGAGTACAAGCTAGC<br>HR template: PCR product: amplification of plasmid **#2120** [Seh1 intron8/exon9 HR-mAID-EGFP-mSeh1 exon9 UTR (gRNA resistant)-HR] with primers AV48/AV49 (for clone D2) OR **#2120** digested with SnaBI and HindII (clone E9) | *Seh1-mAID-GFP* #1 | E9 | Alleles 1 and 2: Seh1–mAID-EGFP<br>(only one band detected and sequenced, corresponding to the AID predicted allele).<br>Note that both alleles carry a 207 bp endoduplication in intron 8, 28 bp before exon 9 that however did not affect Seh1 expression compared to *Seh1-mAID-GFP* #2 cells | 40 Chr (>86%) |
| | | *Seh1-mAID-GFP* #2 | D2 | Only one band detected by PCR<br>Seh1–mAID-EGFP as predicted | 40 Chr (>76%) |

| Table S2. Plasmids used in this study | | |
|---|---|---|
| **Plasmid** | **Source** | **Identifier** (Doye lab) |
| pU6_CBh-Cas9-T2A-mCherry Tigre 3UTR | From P. Navarro Gil and N. Festuccia (Festuccia et al., 2019) | #2061 |
| pTIGRE-CAG-GFP*mNup133dMid | This paper | #2102 |
| pTIGRE-CAG-GFP*mNup133FL | This paper | #2103 |
| Cas9HF-Cherry-1gRNA-degron-Nup133 | This paper | #2109 |
| CMV-EGFP-IntronVariant1-mAID-hSeh1cDNA | This paper | #2108 |
| Cas9HF-Cherry-1gRNA-degron-Seh1Cterm | This paper | #2115 |
| mAID-EGFP-mSeh1-exon9-UTR | This paper | #2120 |
| pCAG-GFP*-miniNup210L (SP-GFP*-TM-Cter) | This paper | #2130 |

Plasmids used in this study were either previously published or generated using standard molecular cloning techniques as previously described in (Gonzalez-Estevez, Verrico et al., 2021). Plasmid maps are available upon request to V. Doye and plasmids will be shared subject to the signature of a UBMTA. See details about GFP* in the legend to Figure S2.

| Table S3. gRNA sequences used in this study | | |
|---|---|---|
| **Identifier** | **Sequence** | **Source** |
| sg-TIGRE | ACTGCCATAACACCTAACTT | (Gonzalez-Estevez, Verrico et al., 2021) |
| gRNA-degron-Nup133 | GTTCGCGGAGAGGAGACGCT | This paper |
| gRNA-Seh1Cterm | AGCTGAGTACAAGCTAGC | This paper |

| Table S4. Primers used to generate homology-directed repair templates for *Nup133-degron* and *Seh1-degrons* | | |
|---|---|---|
| **Name** | **Sequence** | **Source** |
| CO69 (FW, plasmid #2108) | CCTCAGGTGTTCAAGCTCCGGGCGCGCGAGGTTCTCGCTATTAGCCCGCGAGTGCCGCTTCCTCCACGCTCTCTGCAAACATGGTGAGCAAGGTAAGTATC | This paper |
| CO34 (RV, plasmid #2108) | GTGGACGTGGGCCCGATCCCGACTAGCGGACCGCGTCGGGTCCCCGGCCCTGGGGTTCGCGGGCTGGAGACGGACGGAAAGGATCTGAGTCCGGATTTATA | This paper |
| AV48 (FW, #2120 plasmid) | GAACAAATTATTTTATGAAGGAAAGCATAGTAGAGTTAATTTTTAAAAATCTGGTTTTAGGTTACAGCTTTAGTTCTGTGTTATTTTCTTCCATAAATAGC | This paper |
| AV49 (RV, #2120 plasmid) | GGCTGACTAGTACAAAAGTTATATACACTGTCACTTTAAAGGCCTTTTGGACTGTGTGTAGTAGTGAACGGGCTGCTGGTGCATCTTGGAAGAGATCAAAC | This paper |

**Table S5: qPCR primers used in this study**

| Name | forward | reverse | Identifier (Doye lab) # |
|---|---|---|---|
| TBP | GAAGAACAATCCAGACTAGCAGCA | CCTTATAGGGAACTTCACATCACAG | 11/12 |
| Nup133-Nter (exons 4-6) | GATTTGGTGGCCCTGTCTTA | GAAACTTCCTCCCTGCACTG | 3/4 |
| Nup133-Mid (exons 13-14) | GACAAGGCCGTGACTCAGAT | CAAGCCGACTTGGTGAAGGA | 330/331 |
| Oct4 | TGCCCAGCATCACTATTTCA | GAAGCGACAGATGGTGGTCT | 17/18 |
| Nanog | TTGCTTACAAGGGTCTGCTACT | ACTGGTAGAAGAATCAGGGCT | 43/44 |
| Sox1 | TGGGTCTCAGAAGGAGGATG | TGGGATAAGACCTGGGTGAG | 23/24 |
| Pax6 | GGGAAAGACTAGCAGCCAAA | TGAAGCTGCTGCTGATAGGA | 336/337 |
| Lhx1 | CTTTGCAGCTACACCCAAGC | CTTGGAGCGTCGATTCTGGA | 440/441 |
| Acta2 | GAGAAGCCCAGCCAGTCG | CTCTTGCTCTGGGCTTCA | 168/168 |
| Nup210L | AGCACTCAATGCTCACGACA | GTTGATGCCAGCACAGCAAA | 215/216 |
| Nup153 | AAGAAAGCCGACAGTGAGGA | TTTGCTGCACCTTGATCAGT | 5/6 |
| Ddx3y | CAATTTTGATTTGCCAAGCG | TTTGTGATGTTCAAATTCCTCTCA | 549/550 |
| Eif2s3y | ATTTGGTGAAAGAAAGCCAGG | GGAGCTCCTTCGGCTACTG | 545/546 |
| Wfikkn1 | GGAAGCCATCCTGGCATGT | CGCACAGTCCTGGTCCC | 434/435 |
| Cyp26a1 | AAGCTCTGGGACCTGTACTGT | CTCCGCTGAAGCACCATCT | 561/562 |
| Igfbp3 | TCAATGTGCTGAGTCCCAGA | TGTCCACACACCAGCAGAAG | 555/556 |
| Nuggc | CATTCCAGGCACAGGAGACT | TCATGGGTCTTTCCTCCAGA | 553/554 |
| T (Brachyury) | CTGGGAGCTCAGTTCTTTCG | GTCCACGAGGCTATGAGGAG | 67/68 |
| Magohb | CCGGACGGGAAGCTTAGATA | AGAGCGTCGTCCTCTTTTGT | 253/254 |
| Alpn | CTCTGGCTCTCCTTGACTGC | GCGCATGCTTCCTTCTTCTA | 293/294 |
| Rasgrp1 | ACCGGATCATCATCTCCTCA | AATTCTTTTCCAGGGCATCC | 297/298 |

**Table S6: Antibodies used in this study**

| **Primary Antibodies** | **Usage** | **Concentration** | **Identifier** (Doye lab) | **Source /reference** |
|---|---|---|---|---|
| Mouse monoclonal antibody anti-Nup153 (SA1) | IF | 1/5 | #11 | From B. Burke (Bodoor et al., 1999) |
| Rabbit polyclonal antibody anti-Tpr | IF | 1/200 | #158 | Abcam (ab84516) |
| Rabbit monoclonal anti Nup98 C39A3 | IF | 1/20 | #236 | Cell signaling (#2598) |
| Rat monoclonal anti-mouse Nup133 antibody (clone 9C2H8) | IF | 1/100 | #74 | Doye lab (Berto et al., 2018) [2] |
| Rat monoclonal anti-mouse Nup133 antibody (clone 3C11G6) | WB[1] | 1/10 | #75 | Doye lab (Souquet et al., 2018) [2] |
| Rabbit monoclonal antibody anti-Nup133 (EPR10809) | WB[1] | 1/500 | #295 | Abcam (ab181355) |
| Rabbit polyclonal antibody anti-Seh1 | WB | 1/1000 | #297 | Abcam (ab218531) |
| Mouse anti-gamma-tubulin | WB | 1/2500 | #3 | Abcam (ab11316) |
| | | | | |
| **Secondary antibodies** | | | | |
| Cy™5 AffiniPure Donkey anti-mouse | IF | 1/500 | #504 | Jackson ImmunoRes. 715-165-151 |
| Cy™5 AffiniPure Donkey anti-rat | IF | 1/500 | #561 | Jackson ImmunoRes. 712-035-152 |
| Cy™3 AffiniPure Goat anti-rabbit | IF | 1/500 | #519 | Jackson ImmunoRes. 111-165-144 |
| Peroxidase AffiniPure Donkey anti-rabbit | WB | 1/1500 | #499 | Jackson ImmunoRes. 711-035-152 |
| Peroxidase AffiniPure Goat anti-mouse | WB | 1/5000 | #515 | Jackson ImmunoRes. 115-035-068 |
| Peroxidase AffiniPure Goat anti-ratCy™5 AffiniPure Donkey Anti-Rat | WB | 1/10000 | #523 | Jackson ImmunoRes. 112-035-167 |

[1] The rat monoclonal anti-mNup133 antibody (#75) was used in Figs 2B, 4C and S3B. The rabbit antibody (Abcam) was used in Figures 4B.

[2] 9C2H8 and 3C11G6 anti-mNup133 monoclonal antibodies are now commercially available through Millipore. The indicated dilutions may not apply to this commercial source.

Validation of the anti-Nup153 and rat anti-Nup133 monoclonal antibodies is described in the indicated publications. Information on the commercial antibodies used in this study is provided by the manufacturers. In addition, the commercial Seh1 antibody was previously validated by western blot using corresponding KO mESCS (Gonzalez-Estevez et al. 2021).

**References cited in Supplemental Materials and Methods:**


Berto, A., Yu, J., Morchoisne-Bolhy, S., Bertipaglia, C., Vallee, R., Dumont, J., Ochsenbein, F., Guerois, R., Doye, V. (2018). Disentangling the molecular determinants for Cenp-F localization to nuclear pores and kinetochores. EMBO Reports. 19, e44742.

Bodoor, K., Shaikh, S., Salina, D., Raharjo, W. H., Bastos, R., Lohka, M., Burke, B. (1999). Sequential recruitment of NPC proteins to the nuclear periphery at the end of mitosis. J. Cell Sci. 112, 2253-2264.

Festuccia, N., Owens, N., Papadopoulou, T., Gonzalez, I., Tachtsidi, A., Vandoermel-Pournin, S., Gallego, E., Gutierrez, N., Dubois, A., Cohen-Tannoudji, M., Navarro, P. (2019). Transcription factor activity and nucleosome organization in mitosis. Genome Research. 29, 250-260.

Gonzalez-Estevez, A., Verrico, A., Orniacki, C., Reina-San-Martin, B., and Doye, V. (2021). Integrity of the short arm of the nuclear pore Y-complex is required for mouse embryonic stem cell growth and differentiation. J. Cell Sci. 134, jcs258340.

Harkins, H.A., Page, N., Schenkman, L.R., De Virgilio, C. Shaw,S., Bussey, H.,and Pringle, J.R. (2001) Bud8p and Bud9p, proteins that may mark the sites for bipolar budding in yeast. Mol. Biol. Cell 12,2497-518.

Guzzardo, P. M., Rashkova, C., Dos Santos, R. L., Tehrani, R., Collin, P., Bürckstümmer, T. (2017). A small cassette enables conditional gene inactivation by CRISPR/Cas9. Scientific Reports. 7, 16770.

Natsume, T., Kiyomitsu, T., Saga, Y., Kanemaki, M. (2016) Rapid Protein Depletion in Human Cells by Auxin-Inducible Degron Tagging with Short Homology Donors. Cell Reports. 15, 210-218.

Selfridge, J., Pow, A.M., Mcwhir, J., Magin, T. M., Melton, D. W. (1992) Gene Targeting Using a Mouse HPRT Minigene/HPRT-Deficient Embryonic Stem Cell System: Inactivation of the Mouse ERCC-1 Gene. Somatic Cell and Molecular Genetics. 18, 325-336.

Souquet, B., Freed, E., Berto, A., Andric, V., Audugé, N., Reina-San-Martin, B., Lacy, E., Doye, V. (2018) Nup133 Is Required for Proper Nuclear Pore Basket Assembly and Dynamics in Embryonic Stem Cells. Cell Reports. 23, 2443-2454.

Tsien, R.Y. (1998) The green fluorescent protein. Annu. Rev. Biochem. 67, 509-544